Development of a sensor and measurement platform for water quality observations: design, sensor integration, 3D printing, and open-source hardware

Nicholas John Kinar (n.kinar@usask.ca)
University of Saskatchewan https://orcid.org/0000-0002-4284-0601
Markus Brinkmann
University of Saskatchewan

Research Article

Keywords: water quality, sensors, IoT, 3D printing, open source

Posted Date: April 22nd, 2021

DOI: https://doi.org/10.21203/rs.3.rs-449278/v1

Version of Record: A version of this preprint was published at Environmental Monitoring and Assessment on February 22nd, 2022. See the published version at https://doi.org/10.1007/s10661-022-09825-9.

Development of a sensor and measurement platform for water quality observations: design, sensor integration, 3D printing, and open-source hardware

Environmental Monitoring and Assessment

N. J. Kinar[1,2*] and M. Brinkmann[1,2,3,4*]

Keywords: water quality, sensors, IoT, 3D printing, open source

[1]Smart Water Systems Lab, University of Saskatchewan
[2]Global Institute for Water Security, University of Saskatchewan
[3]School of Environment and Sustainability, University of Saskatchewan
[4]Toxicology Centre, University of Saskatchewan

*Corresponding authors:

Dr. Nicholas Kinar
11 Innovation Blvd
Saskatoon SK S7N 3H5 Canada
Phone: +1 305 966 2092
E-mail: n.kinar@usask.ca

Dr. Markus Brinkmann
Toxicology Centre, 44 Campus Drive
Saskatoon SK S7N 5B3 Canada
Phone: +1 306 966 1204
Email: markus.brinkmann@usask.ca

Abstract

A measurement and development platform for collecting water quality data (the WaterWatcher) was developed. The platform includes sensors to measure turbidity, total dissolved solids (TDS), and water temperature as variables that are often collected to assess water quality. The design is extensible for research and monitoring purposes, and all design files are provided under open-source permissive licenses for further development. System design and operation are discussed for illustrative purposes. A block diagram indicates elements of mechanical, electrical, and software design for this system. The mechanical assembly used to house circuit boards and sensors is designed using 3D printing for rapid prototyping. The electronic circuit board acts as a carrier for an Arduino 32-bit microcontroller board and an associated cellular module along with a GPS for geolocation of water quality measurements. The cellular module permits data transfer for Internet of Things (IoT) functionality. System operation is set up using a command line interface (CLI) and C++ code that allows for calibration coefficients and human-readable transfer functions to be defined so that sensor voltages are related to physical quantities. Data are cached on a secure digital (SD) card for backup. The circuit was calibrated, and system operation assessed by deployment on an urban reservoir. Biogeochemical cycles were identified in the collected data using spectrogram and semivariogram analyses to validate system operation. As a system with hardware and software released under an open source license, the WaterWatcher platform reduces the time and effort required to build and deploy low-cost water quality measurement sensors and provides an example of the basic hardware design that can be used for measurements of water quality.

Acknowledgements

Thank you to Prof. John Pomeroy, Director of Global Water Futures and the Smart Water Systems Lab, for supporting this research. Thanks to the staff of the Toxicology Centre for testing support and Mr. Alistair Wallace (SWSL) for some assistance with the mechanical assembly. We thank and acknowledge Environment and Climate Change Canada (ECCC) for providing precipitation data and Digikey Incorporated (Thief River Falls, Minnesota, USA) for providing electronic parts and permission to use photographs for Figure 1 of this paper.

Introduction

Water quality refers to the properties of water that influence biological systems (Karr and Dudley 1981). This includes civil engineering (Brabec et al. 2002) and toxicological applications (Vlaming et al. 2000), where characteristics of water are measured for determination of hazards related to potable water use and ecosystem services. Pollutants and toxins from sewage, industrial waste, and stormwater runoff enters rivers and streams (Deblonde et al. 2011), potentially modifying biogeochemical cycles. Nitrogen and phosphorus from agricultural and domestic uses of fertilizers stimulate the growth of algae and other microorganisms, decreasing oxygen levels in water and causing eutrophication (Conley et al. 2009). In some urban environments, runoff enters storm sewers (DeFilippi and Shih 1971) that convey solutes to stormwater retention ponds (Borne 2014) and surface hydrological systems (Marsalek 1991). Due to an increase in urbanization and a decrease in infiltration associated with a reduction of soil permeability, stormwater discharge has increased in recent decades, and water quality has decreased due to a concomitant increase in transported chemicals and ions (McGrane 2016).

In light of these aforementioned stressors, water quality is one of the central factors determining ecosystem functionality and the sustainability of human activities (Gleeson et al. 2020). Despite the importance of collecting water quality data, traditional techniques for sampling are prohibitive of early detection of changes (Madrid and Zayas 2007). This is because manual sampling involves the collection of data (either directly using handheld probes, or from lab analysis of samples) from a field site by human investigators, which increases cost and limits throughput. Therefore, there is a need for methods that allow for collection of data at higher temporal and spatial resolutions.

The Internet of Things (IoT) concept involves the use of embedded computing devices to collect and transfer data over a network for automation of observations and the associated display and analysis of data in near real-time (Ng and Wakenshaw 2017). IoT devices are designed to be ubiquitous and communicate over WiFi (L. Li et al. 2011), cellular (Mangalvedhe et al. 2016), or mesh radio networks (Yu et al. 2017) to transfer data between devices and systems (Suo et al. 2012). The collected datasets are used for decision-making (Lee et al. 2013), process control (Prathibha et al. 2017) or environmental modelling applications (Wong and Kerkez 2016). IoT intends to provide adequate spatial and temporal coverage to obtain data useful for predictions and forecasts.

Water quality data have been collected using Internet of Things (IoT) technologies. Water quality sensors have been deployed to monitor river (Chen and Han 2018) as well as inland water and maritime environments (Prasad et al. 2015), and have also been deployed on a robotic boat to obtain spatial estimates of water quality (T. Li et al. 2017). Commercial IoT sensor platforms have been utilized for this purpose (Wong and Kerkez 2016). Commercial devices are relatively expensive, and the use of commercial hardware can result in vendor lock-in (Willocx et al. 2018), resulting in the need to upgrade devices when deprecated by the manufacturer (Pal et al. 2018), and supporting the necessity of paying for access to software and associated technical support required for system functionality (Boehm and Abts 1999).

Water quality measurement systems have been implemented using experimental platforms involving a Raspberry Pi (Chandrappa et al. 2017; Gopavanitha and Nagaraju 2017; Raju and Varma 2017; Vijayakumar and Ramya 2015) and electronic evaluation kits (Das and Jain 2017; Geetha and Gouthami 2017; Myint et al. 2017). However, the Raspberry Pi filesystem can become corrupted over time, resulting in system failure (Nadaf and Bonal 2019) and many evaluation kits are not intended for use in actual products due to long-term reliability (Texas Instruments 2011).

The Arduino platform provides easy-to-use hardware and software with an open source license (Badamasi 2014; Sarik and Kymissis 2010). Open-source hardware allows for design re-use and innovation and thereby enables a better understanding of system functionality due to the availability of schematics and associated design documentation (Fisher and Gould 2012; Pearce 2012). Open-source

software also allows for code reuse: since the source code is available, software functionality can be easily extended and modified (Bonaccorsi and Rossi 2003; Fitzgerald 2006), especially when permissive licenses such as the GNU GPL allow for freedom of use (Di Penta et al. 2010). Arduino-based platforms have been used to collect water quality data and exchange data over WiFi (Chowdury et al. 2019; Parameswari and Moses 2019; Pasika and Gandla 2020), Zigbee (Encinas et al. 2017; Kamaludin and Ismail 2017; Pranata et al. 2017), LoRa (M. Saravanan et al. 2017) and cellular (Moparthi et al. 2018; K. Saravanan et al. 2018) networks. However, most of these water quality measurement projects, although based on open-source hardware and software technologies, do not provide the complete design under a permissive open-source license. This does not allow previous research work to be easily re-used to create additional systems.

This paper introduces a floating water quality measurement platform with open-source hardware and software that can be utilized to develop water quality measurement applications without the need to replicate some common system components. This platform is named the "WaterWatcher." The hardware of the WaterWatcher platform is based around a custom electronic circuit that serves as a carrier printed circuit board (PCB) for an Arduino microcontroller. The microcontroller is interfaced to a cellular communications module. A 3D-printed enclosure is used to house the circuit board and provide a mounting platform for solar panels that power the circuit and charge an on-board Lithium-ion battery. The 3D-printed enclosure, circuit board design files, and Arduino code are provided as an associated download licensed under permissive open-source licenses. The WaterWatcher platform is intended to enable future innovation and development of water quality measurements by the scientific community. This paper is also intended for educational or teaching purposes and serves as an overview of the ideas and technology for water quality measurements.

Materials and methods

Block diagram and system operation

Electronic sensor systems for observations of water quality have common features as identified by the block diagram of the WaterWatcher system (Figure 1). There are three canonical sensors attached to the system: turbidity, total dissolved solids (TDS), and temperature. Additional sensors for chemical measurements can be eventually added. A 3D model of the PCB for this platform implementation is shown in Figure 2a, whereas the assembled PCB is shown in Figure 2b.

An analog frontend provides signal conditioning for voltage inputs from sensors that measure turbidity and TDS. These two sensors are utilized for water quality estimates by many studies and were therefore provided for use in this development platform. Temperature influences TDS determined using an empirical sensor calibration curve (Rusydi 2018) and temperature also influences water chemistry kinetics (Gholizadeh et al. 2016; Paul et al. 2019), so a temperature sensor should always be included.

Turbidity is related to particulate matter from erosion, sewage, geological, and biological sources. The particulate matter present during periods of higher turbidity reduces photosynthetic production, increasing absorption of solar radiation and water temperatures (Davies-Colley and Smith 2001) and decreasing dissolved oxygen levels (Henley et al. 2000). Turbidity levels are used to assess the quality of drinking water since higher amounts of particulate matter can provide environments for pathogens (Farrell et al. 2018). Electronic turbidity sensors are usually optical and relate light extinction to Nephelometric Turbidity Units (NTU) (Davies-Colley and Smith 2001).

Total dissolved solids (TDS) are a measure of chemical and biological substances that exist as molecules, ions, or colloids in the water. Higher levels of TDS are related to greater amounts of dissolved

substances (Weber-Scan and Duffy 2007). Electronic TDS sensors relate parts-per-million (ppm) TDS to electrical conductivity (Ivan et al. 2011).

Inputs can also be added for additional sensors for measurement of water temperature gradients at depths below the water surface. These additional sensor inputs can be digital and attached to a multidrop bus. The WaterWatcher uses the 1-wire bus (Dudak et al. 2018) where multiple sensors are attached to the same wired connection and each sensor is associated with a unique address. The temperature sensor used for the WaterWatcher is digital as an application-specific integrated circuit (ASIC) since the use of an ASIC decreases complexity.

The main microcontroller enables periodic sampling of analog and digital inputs. Interfaced with a cellular communications module, the microcontroller periodically sends data to a base station or server. However, since radio frequency (RF) communications are not always reliable due to topographic and environmental effects or infrastructure failure, there must be a means for data to be locally cached. This enables data to be retrieved later in the field or to be re-sent to the server at a time when the circuit can communicate with a network. A ubiquitous flash memory device for storing data is an SD card that is readily available from commercial sources. The SD card can be extracted and inserted into a reader to transfer data to a computer for analysis. A USB bus allows for Machine-2-Machine (M2M) communications where system operation is configured using a computer.

A GPS receiver module provides geographic location and elevation data. Although the water quality measurement platform might be installed at a stationary location in, e.g., a stormwater retention pond or reservoir, GPS measurements allow for WaterWatcher devices to be located on a web map interface or to be tracked for property inventory purposes. Moreover, if the water quality measurement platform is towed behind a boat or set adrift in a river or reservoir, geographic location can be related to spatial changes in water quality.

The system requires DC power and cannot be easily interfaced to AC power via a converter since water quality devices are often placed in bodies of water at remote locations and field sites. The WaterWatcher therefore requires a battery charger system interfaced to solar panels. To reduce the overall mass of the system, the batteries are Li-ion cell chemistry, but a protection circuit is also required to limit the rate of charge, reduce overcharge and over-discharge, and also ensure that a battery fault does not cause an explosion or fire (Salerno and Korsunsky 1998).

To protect the WaterWatcher circuit from water ingress and to provide a mounting platform for the water quality sensors, a mechanical enclosure is required. This mechanical enclosure can be created from plastic. To allow for rapid prototyping and modification (Oropallo and Piegl 2016), the enclosure is 3D-printed for prototyping and low-volume applications.

At the time of writing, the cost of mechanical parts and electronic circuit boards is under $1,000 CND. The WaterWatcher can thereby be created at a fraction of the cost of commercial water quality sensor platforms.

Mechanical design

The mechanical design for the WaterWatcher floating water quality sensor platform is shown as an exploded diagram (Appendix A) and a computer rendering as Figure 3a. Although buoy design can be conducted with specialized software packages that allow for modeling of wave interaction with the structure (García et al. 2018), we used a standard mechanical CAD system to maximize reproducibility and design sharing since this type of software is more readily available to researchers.

Mechanical design calculations are performed separately in accordance with engineering principles, and since the platform is intended for use at inland water locations, it is less important to model wave action thoroughly using numerical models. Design calculations ensure that the platform has

a high enough metacentric height to guarantee static stability and sufficient period of roll to prevent internal damage of wiring during wave action. These are design goals nominally associated with marine structures (Terada et al. 2019).

Although a proprietary CAD system was used for the design, STEP files are also provided in a vendor neutral format for use with open-source CAD software packages or for 3D printing. All assembly pieces shown on the diagram were printed on an engineering-grade 3D printer (Fortus F370, Stratasys Inc) using acrylonitrile styrene acrylate (ASA) plastic. ASA plastic was chosen since this material is UV-stabilized for outdoor locations and is similar in hardness to ABS plastic. Support material was used by the 3D printer to create holes. After removal of the support material in a detergent bath, the holes were functional and precisely located as specified by the mechanical CAD design. This eliminated the need for drilling of holes after 3D printing and reduced a step of the manufacturing process. The following paragraphs indicate alphabetic identifiers on the diagram provided in Appendix A.

A bottom rudder (A) is fastened to a circular inner assembly (B) that provides a conduit for wires and a mounting point for the three basic sensors that measure turbidity, TDS, and temperature. Analogous to rudders on boats (Liu and Hekkenberg 2017), the rudder allows the sensor platform to travel with the flow in a river or stream. The rudder can be turned to different cardinal directions by removing the fasteners and updating the 3D model. Additional holes created in the circular inner assembly (B) can accommodate wires for additional sensors.

The circular inner assembly (B) is attached by fasteners to two carbon fiber (C) plates glued between polyethylene foam sheets (D, E). The edges of the sheets are rounded to prevent mechanical disaggregation of the sheets if a collision occurs. This distributes the collision force over a larger surface area.

Regions of the bottom foam sheet (D) were removed to ensure that the inner assembly and the carbon fiber plates are flush with the foam sheet surface. The removal was done by hand, but a CNC machine can also be used. The removal of material ensures that the foam sheets can be glued together without a gap. The carbon fiber plates (C) were glued together using a marine adhesive epoxy.

The platform is assembled in a stacked fashion by threaded rods (F) inserted into holes created in the circular inner assembly. The rods are held in place by nuts inside of the circular inner assembly. A cap (G) protects against water ingress and provides a seating plane for the upper part of the assembly. A hole is created through the top of the cap to admit wires from the sensors.

A plate (H) with holes is placed on top of the polyethylene foam sheets. The plate is held in place by the threaded rods and provides a mounting location for GPS and cellular antennas. Conduits for the coaxial cables connected to each antenna are created in the foam. The plate was divided in half to not exceed the lateral build dimensions of the available 3D printer. This entails printing the single plate as two separate plastic pieces that are later joined together.

A plastic parallelepiped (I) is placed on top of the threaded rods. Holes on opposite sides of the parallelepiped allow for the coax cables from the GPS and cellular antennas to be brought into the internal cavity and connected to the PCB (Figure 2). The sides of the parallelepiped are recessed to hold solar panels (J) glued to the sides using a marine epoxy. The solar cells are placed on all sides of the parallelepiped to maximize electrical power output.

Another cap (K) and a similar plastic parallelepiped (L) are placed on top of the lower parallelepiped (I). The threaded rods (F) are used to stack together the two parallelepipeds. The top parallelepiped has threaded inserts to admit bolts that fasten on a lid (M). Integrated into the lid is a holder for the PCB (N). The PCB is bolted to the holder (Figure 2b) along with a RF (radio frequency) bias tee module to provide power to the active GPS antenna. The top of the lid has a holder for a solar-powered strobe light (O). The strobe light (O) is inserted into the holder and glued in place.

During and after assembly, a silicone sealant was applied to waterproof portions of the design to protect against water ingress. A sprayable sealant was applied to all surfaces for weatherproofing and to

fill in small gaps in the plastic. Since ASA tends to shrink after printing, the sealant further waterproofed the mechanical assembly.

The total height of the assembly from the bottom of the rudder to the top of the strobe light is 36 inches (91.4 cm). The maximum width of the foam is 18 inches (45.7 cm) and the maximum length is 24 inches (61 cm). These dimensions indicate that the WaterWatcher is a compact platform for water quality measurements, and it has been successfully deployed and retrieved by a single person from a canoe.

Images of assembly are available for download. The images are licensed under a permissive license and serve as an example of how the WaterWatcher was assembled.

Electrical design

Appendix B provides schematics for the circuit. Two analog inputs (A0 and A1) allow for digitization of voltages from turbidity and TDS sensors. The analog inputs are connected to microcontroller port pins set up as analog inputs. The microcontroller has an integrated 12-bit ADC for digitization of voltages and a nominal resolution of 0.8 mV for a configured internal voltage reference of 3.3 V.

Op-amp U23A is configured as a unity gain buffer to provide a high-impedance input for the turbidity sensor. A voltage divider comprised of resistors R35 and R36 scales the maximum sensor voltage to be less than 3.3V as the input to a microcontroller port pin configured as an analog input. Op-amp U23B is another unity-gain buffer that provides a low driving impedance to the analog input port pin so that the accuracy of the measurement is not affected. Diode D3 is a low-capacitance electrostatic discharge (ESD) protection diode.

Since the TDS sensor voltage output is pre-processed using circuitry on a small PCB provided with the sensor module, the driving impedance is low enough to directly interface this sensor to the analog input. An ESD diode D4 also protects the input. Similar diodes are also used for ESD protection on other inputs shown throughout the schematic.

A 1-wire multidrop bus (D0) is implemented using microcontroller GPIO bit-banging. A 1-wire temperature sensor to measure water temperature is attached to this bus. The 1-wire bus has multidrop communications, where each sensor on the bus has a unique serial number and is enumerated using a bus protocol. As per the name, only one wire is used for the bus and another for electrical ground (GND) (Eisenreich and DeMuth 2003, pp. 345–369). Similar to other digital busses, the maximum number of devices added to the bus is limited only by wire connection resistance and capacitance allowing for dozens of sensors to be added. Linear regulator U22 provides power to the temperature sensors.

Headers J1 and J2 connect two 3.7 V Li-ion batteries with a capacity of 2 A hr in series to provide a 7.4 V nominal source. U3 is an overvoltage protection IC that also performs cell balancing to ensure that the voltages of each battery are approximately equal during charging and discharging. This increases efficiency and battery life and protects against thermal runaway that can create a fire hazard. U1 and U2 are field effect transistors (FETs) with integrated charge pumps and current-limiting circuitry that limits the maximum bi-directional current flow to the battery. U4 is a battery monitor with a charge integrator that reports the battery state-of-charge. An ADC integrated into U4 is connected to header J3 to provide another ADC input (identified as A2). ADC input A2 can be used to measure the voltage output of another sensor.

The battery charger U5 provides maximum power point tracking (MPPT) for solar panels to ensure that the batteries are efficiently charged when enough solar energy is present. Each solar panel has a 9 V nominal open circuit voltage with a current of 220 mA for a maximum output power of approx. 2 W. Connecting the cells in the configuration shown results in a maximum 18 V open circuit voltage

with a maximum current of 880 mA for a maximum output of approx. 16 W. Diodes D7 and D9 allow for the solar panels to power the circuit directly or when the battery is dead or not present.

The power supply built around U17 utilizes a switch-mode topology with inductor L4. This power supply is more efficient than a linear regulator to provide a 5 V main system rail. The input to U17 is filtered using an LC filter to reduce the effects of electromagnetic interference (EMI). U18 is a FET with integrated charge pump that acts as a switch to turn on and off the external 5 V rails that provide power to the sensors. This conserves current since the 5 V rail is only turned on during the time of a measurement.

U7 is a GPS module. Linear regulators U8 and U9 provide a quiet power supply to the GPS to reduce noise from the 5 V main system rail. U8 is the main linear regulator whereas U9 serves as a battery backup for the GPS, reducing the time to first fix (TTFF) when the main supply to U8 is turned off between measurements to conserve battery power.

U20 is a unique serial number that identifies each circuit board. Linear regulator U21 provides current to a real-time clock (RTC), a port expander (U24), and a buffer (U15). The RTC provides a timestamp for each observation and allows for measurements to be taken on a schedule ranging from minutes to hours. The port expander samples battery state and is used to determine if there is a battery fault or if the battery is charging.

Buffer U15 protects against current flow to the GPS module when it is powered down and serves as a Faraday shield (Zumbahlenas 2008, pp. 845–846) for reduction of logic noise from the main processor module port pins configured as a TTL serial port. The Arduino MKR GSM 1400 module (U14) is based around a 32-bit ARM processor interfaced to a cellular chipset for IoT connectivity. A SIM card is inserted into the module. For this reference implementation, we initially used the Hologram.io cellular platform to exchange data: the platform is inexpensive, provides a REST API for implementation of web services, and is supported for use with the Arduino ecosystem. Later experimentation utilized a web server with a web framework to store data in a custom database.

The main processor module U14 is interfaced to an SD card by a serial peripheral interface (SPI) bus. The SD card is operated in SPI mode in lieu of a 4-bit parallel bus since the main processor module lacks a hardware SD card master but analogous to most microcontrollers incorporates an SPI master. For power-down between measurements, linear regulator U16 is turned off by the main processor module. To prevent current flow between the main processor module port pins and the SD card during power-down, all port pins connected to the SD card are set as inputs.

A micro-USB connector on the main processor module U14 serves to implement a USB serial port that provides a command line interface (CLI) for the WaterWatcher. The CLI allows for the sampling platform to be configured and tested.

Software design

The software design for the WaterWatcher is based around the Arduino platform for reproducibility and to reduce the amount of effort required for modification. Although existing Arduino software libraries were used as required, custom code was also created for the RTC U19, port expander U24, battery monitor U4, and serial number integrated circuit U20. This ensured flexibility in the context of the application. The SD card library required for reading and writing the FAT filesystem was FatFs (version 86604) with a custom media access interface written specifically for SPI communications. This custom implementation was chosen over Arduino-provided SD card libraries to ensure that high-capacity exFAT cards could be used as interfaced to the SPI bus. The use of exFAT cards allows for years of data to be stored on a single card.

An example of the setup is provided as C++ code in Table 1 as an Arduino sketch file. Arduino code requires two functions: setup() and loop(). The setup function initializes the hardware, whereas the loop function is an infinite loop that checks the state machine logic implemented by the code.

An instance of the WaterWatcher class is created as a global object in the main sketch. The setup is implemented by a call to class member setup(). The check of internal state is implemented by a similar call to class member function checkState() in the loop() function. These are the only required functions in the user code and the WaterWatcher class encapsulates functionality. Additional functionality, such as the sampling interval, is set using the Command-Line Interface (CLI).

The basic structure of the code in Table 1 can be modified if required to add additional functionality. The code demonstrates how the WaterWatcherOptions sub-class is inherited from the associated base class to override transfer functions that provide processed analog outputs relating a voltage to a physical measurement such as turbidity or TDS. The processed water temperature can also be adjusted based on calibration. The analog channels are set to sample or not to sample during a measurement.

Table 2 lists commands entered using the CLI when the WaterWatcher is attached to a host computer via the USB cable. The commands allow for various sub-systems to be read, specify whether the data is to be sent over cellular, and indicate whether the system is to enter a power-saving mode. CLI arguments are separated by spaces. As indicated in the table, some settings can be saved into non-volatile flash memory using the *write-flash* command. These settings are reloaded after each power cycle. The total length of non-volatile strings saved into flash memory is limited by the amount of flash memory available for storage.

Data can be stored on the SD card in JSON (JavaScript Object Notation) format. CSV (Comma-Separated Values) format has been nominally used by dataloggers and is not self-documenting. JSON format is widely used for data interchange and is human-readable (Bassett 2015). Each object is clearly identified, unlike CSV that relies on additional metadata to identify the contents of each column. Most programming languages (including R and Python) can easily parse JSON and convert this format to CSV or other table-based formats. The code can be modified to store data in CSV or JSON formats.

Laboratory testing and calibration

The WaterWatcher was placed into a tank at the Toxicology Centre, University of Saskatchewan (Figure 3b). Waves were created in the tank by displacement to test the buoyancy and stability of the platform (Figure 3c). A video of the wave testing experiment is provided in the associated downloads for this paper.

A commercial multiparameter sonde equipped with turbidity and TDS sensors (EXO2, YSI Incorporated, Yellow Springs, Ohio, USA) was also inserted into the tank and used to collect comparison data to relate WaterWatcher sensor voltages to turbidity and TDS. The tank was filled with deionized water and fitted with a standpipe to allow it to overflow. Commercially available coffee whitener and sodium chloride was used to create water with defined turbidity and TDS. After starting the readings, a constant flow of deionized water was used to dilute the colloid and salt. This caused a time-dependent drop in turbidity and TDS following first-order kinetics. All laboratory data were logged to the SD card using a 5-minute sampling interval. The same 5-minute sampling interval was also used for the YSI sonde. Data were collected for approximately 31 hours for a total of 365 samples.

The data were subjected to statistical analysis. Additional plotting and analysis were conducted using the Python programming language and the source code provided for download.

Field deployment

The WaterWatcher was deployed at an urban reservoir (Aspen Ridge Forebay) situated near the Northeast Swale within the municipal boundaries of the City of Saskatoon, Saskatchewan, Canada (Figure 4). The urban reservoir is a pond with engineered storm drain discharge from surrounding neighborhood locations.

The Northeast Swale is a geographical area representative of ecosystem diversity with native grassland, wetlands and rare species that are subjected to increasing urban land use (Shen et al. 2019). The WaterWatcher was anchored to the bottom of the reservoir using coated aircraft cable and a concrete weight. To conserve power, measurements of turbidity, TDS and temperature were collected every 30 minutes, cached on the SD card, and sent via cellular communications to a server.

Results and discussion

Laboratory testing and calibration

The wave-testing experiment (Figure 3c) showed that the platform did not capsize during water turbulence and demonstrated the veracity of the engineering design. Since water ingress was not observed after more than a week of the sensor floating in the tank, we deemed the enclosure sealing and the plastic thickness to be suitable for a waterproof design demonstrating system operation. This does not preclude the possibility of leaks arising over time, or water ingress from total submersion of the WaterWatcher, necessitating the need for maintenance and possible repair between field deployments in a similar fashion to commercial sensors.

As determined from laboratory testing and calibration, Figure 5a shows the relationship between turbidity and voltage as well as the associated model found by curve-fitting. Figure 5b exhibits similar relationships and curve-fitting models related to TDS.

Polynomial curve-fitting was used to smooth the output voltage time series of the WaterWatcher turbidity sensor. The sensor voltage was related to YSI sonde turbidity measurements using polynomial curve-fitting subject to the constraint that the polynomial must be monotonic to model a decrease in turbidity over the time of experiment. This is to ensure that higher output voltages are always correlated with lower turbidities. Since the turbidity sensor measures turbidity by light extinction, lower levels of turbidity will be associated with less light extinction and higher voltages. A univariate spline model was then used to obtain a function relating turbidity sensor output voltage to turbidity (Figure 5a).

After polynomial curve-fitting to initially smooth the output voltage time series of the WaterWatcher TDS sensor, 2D polynomial curve-fitting was used to obtain a function relating the output voltage and water temperature to TDS as measured by the YSI sonde (Figure 5b). The function outputs were corrected for linear offsets to compensate for differences between tank and field observations associated with differences in temperature and fluid mixing processes. Table 3 shows that the Root Mean Squared Difference (RMSD) and Mean Bias (MB) are sufficiently low for the calibration experiments and this indicates that the models adequately characterize relationships between turbidity, TDS and associated voltages.

The theoretical measurement resolution M_r was estimated by converting the microcontroller ADC resolution to NTU and ppm using a transfer function $f(v)$ determined using calibration curve-fitting and by averaging a difference as shown in Equation (1) below over the calibration range of voltages.

$$M_r = \frac{1}{N}\left|\sum_{i=1}^{N}\left[f(v_i) - f(v_i + \Delta v)\right]\right| \quad (1)$$

The v_i is the voltage output of a sensor (turbidity or TDS) measured at a known water temperature, i is an index, and N is the number of discrete data values collected during the experiment. The $\Delta v = 0.8$ mV is the voltage resolution of the 12-bit ADC and $v_1 = \Delta v$. The theoretical measurement resolution M_r for turbidity and TDS was estimated (Table 3). Although the actual measurement resolution will be lower due to circuit noise and sensor circuit errors associated with non-linearities and component variation with respect to time and temperature, this theoretical resolution is likely sufficient to characterize water quality processes at a field site.

The 12-bit resolution is not as accurate as some commercial sensors that may use an ADC with a higher number of bits but digitization of voltages using this resolution can provide an estimate of water quality using low-cost electronics associated with an IoT open-source platform. A higher-resolution external ADC can be added as a circuit board revision for providing more accurate measurements along with additional front-end circuitry such as a programmable gain amplifier (PGA). The PGA can be used to change the amplification of the voltage inputs, thereby allowing for smaller voltages to be measured more precisely.

The CLI allowed for system functionality to be expeditiously tested during calibration. At an indoor location with an average light flux exceeding 5 W m^{-2} from artificial lighting, the microcontroller module was observed to operate using power provided by the solar cells when the batteries were disconnected, demonstrating the efficiency of the switch-mode topology power supply design. However, the Li-ion batteries are still required to provide additional power for reliable GPS, SD card and cellular modem operation. The system current consumption during field deployment is discussed in the sections below.

Field deployment

Figure 6 shows turbidity (a) and TDS (c) time series observations collected by the WaterWatcher at the Aspen Ridge Forebay. To characterize cyclical biogeochemical processes occurring at this location, the time series of turbidity and TDS were subjected to spectrogram analysis (b, d). The spectrogram vertical axis is expressed in Fractional Frequency (FF) ranging from 0 to 0.5, where the high end of this range corresponds with half the sampling frequency as per the Nyquist sampling theorem. The vertical range of the spectrogram plot is set to a maximum of FF = 0.04 for visualization and because most of the Power Spectral Density (PSD) of the signal occurs at a lower frequency than this maximum. Since the sampling interval for field deployment was 30 minutes as 1800 s, the sampling frequency was $\sim 5.56 \times 10^{-4}$ Hz.

The turbidity and TDS time series show diurnal cycles associated with water circulation and mixing in the reservoir that also includes the addition of water from storm sewer systems. The spectrogram corresponding to the turbidity time series (Figure 6b) shows the gradual development of cyclical processes over the time of observation, whereas the spectrogram corresponding to the TDS time series (Figure 6d) shows a reduction in cyclical processes.

An increase in the turbidity and an increase in the TDS occurred concomitant with precipitation events (Figure 6e) near the midpoint of the time series observations. After these precipitation events occur, the turbidity exhibits an increase in cyclical processes, whereas the TDS exhibits fewer cyclical processes. The increase in turbidity and associated cyclical processes in relation to the rainfall event may

have been caused by an increase in water flow to the reservoir and an increase in sediment conveyed to the reservoir by runoff events. Alternately, an increase in TDS and a decrease in associated cyclical processes may indicate an increase in the mixing of water in the reservoir after the addition of runoff from the precipitation events. As expected, water temperature (Figure 6e) exhibits diurnal cycles associated with land surface temperature changes and heating by solar radiation.

The turbidity spectrogram exhibits a dominant cyclical process at FF ≈ 0.004 corresponding to 125 hr or 5.2 days. This indicates a temporal change in reservoir turbidity associated with sediment transport from rainfall events. Alternately, the TDS spectrogram exhibits a dominant cyclical process at FF ≈ 0.02 corresponding to 25 hours, indicating that the TDS has more temporal variability than the turbidity and suggesting the prevalence of diurnal mixing processes in the reservoir.

The battery voltage over the time of field deployment (Figure 6f) ranged between 8.33 V and 5.92 V without any missing data indicating that the system was powered by the battery and solar panels over the time of deployment. Figure 6f also shows discrete battery charging events, demonstrating the operation of the battery charger connected to the solar panels. Battery charging events only occurred when solar power was sufficiently high to provide the required current for charging. The average operating current sourced from the battery over the time of deployment was 64.6 mA, with an increase in current consumption during cellular transmission events, during cloudy days, and at night when current could not be sourced from the solar panels. The average operating current could be reduced using a custom microcontroller in lieu of the Arduino module. This is because the Arduino module and associated electronics has LEDs and the use of lower-efficiency circuit elements that are always powered over the time of deployment.

Figure 7 shows semivariograms computed for the turbidity (a), TDS (b) and (c) water temperature time series. A temporal semivariogram γ indicates autocorrelation over successive time intervals (Haslett 1997). The range is the position on the horizontal plot axis where the semivariogram reaches an approximate plateau referred to as the sill (Goovaerts 1997, p. 89). For the turbidity time series, the range is 9100 min as 6.3 days, whereas for the TDS time series, the turbidity is 8000 min as 5.6 days. The temperature semivariogram exhibits a range of 9200 min as 6.4 days with some diurnal cycles evident at shorter time scales. Since the turbidity, TDS, and temperature time series become less autocorrelated at a time interval of ~6 days, this indicates that manual sampling of water quality data in the reservoir should be conducted at weekly intervals to capture longer-term trends in temporal variability aside from diurnal variability. However, automated measurements are still required to characterize shorter-term biogeochemical cycles. As suggested by cycles in the TDS semivariogram exhibited at time intervals less than the range (Figure 7b), automated sampling is thereby more important to characterize TDS at shorter time scales than turbidity (Figure 7a). Turbidity (Figure 7a) and temperature (Figure 7c) time series have a similar range.

Conclusions

This paper introduced a platform for measurement of water quality with extensible hardware and software. The platform includes sensors that are often used to measure water quality. The mechanical, electrical and software designs are released under permissive open-source licenses to encourage collaboration and reduce the time required to implement a functioning system.

The mechanical design, electronics and software were described for educational purposes. The mechanical design allows for expeditious creation of parts on a 3D printer, enabling parts to be modified as required. For manufacturing of multiple sensor platforms to provide spatial coverage of a city or region, the parts could be created using injection molding. Although the initial setup costs of injection

molding can be high, the cost per part during production is sufficiently low to allow for the creation of a network of multiple WaterWatcher systems.

The electrical design allows for sensors to be sampled and a complete IoT system to be constructed around a microcontroller platform associated with the Arduino ecosystem. This reduces the complexity of updating and editing the code for other associated applications. Moreover, since the basic system functionality can be setup using the CLI, this allows for system operation to be modified and calibration coefficients programmed as human-readable transfer functions without the need for additional computer code to be written. Since the CLI is associated with a virtual serial port, the possibility exists of a computer program with a Graphical User Interface (GUI) and associated hardware being used to automatically set up and calibrate the system after construction. This can allow for multiple sensors to be assembled and quickly tested before deployment.

The WaterWatcher system was calibrated in a lab tank. The calibration process demonstrates the sensor operation and indicates how the system can be calibrated to relate voltages to physical quantities. Despite the low 12-bit resolution of the microcontroller ADC, the WaterWatcher platform can provide estimates of turbidity and TDS that coincide with commercial sensors. The circuit board could be updated in the future with the addition of a higher-resolution ADC and additional sensors that measure water chemistry for additional assessment of pollution and hazards.

The field deployment of the WaterWater demonstrated how the system can be used to collect data at a field location and characterized circuit operation. The time series data was subjected to spectrogram and semivariogram analyses to indicate biogeochemical cycles occurring in the North Swale reservoir.

Multiple WaterWatcher platforms have the potential to create a low-cost network of sensors that report data useful for predictions and forecasts of water quality. The use of open-source hardware and software reduces cost and allows for systems to be easily extended for civil engineering and toxicology applications.

Declarations

Funding

We would like to acknowledge Western Economic Diversification (WED) for funding the Smart Water Systems Lab as well as funding received from the Global Water Futures (GWF) program and the Global Institute for Water Security (GIWS). N.K. received funding from GWF and WED. M.B. received funding through the Natural Sciences and Engineering Research Council of Canada (NSERC) Discovery Grants program.

Conflicts of interest/competing interests

The authors declare no conflicts of interest and no competing interests.

Availability of data and material

Datasets (https://doi.org/10.6084/m9.figshare.14439503.v1) as well as images showing the assembly of the WaterWatcher and video of the wave testing experiment (https://doi.org/10.6084/m9.figshare.14428709.v1) are provided as Figshare downloads and licensed using a permissive license (https://creativecommons.org/licenses/by-sa/4.0/). The hardware as

designed by the authors is licensed using the CERN open hardware license (CERN-OHL, https://www.ohwr.org/cernohl)

Code availability

All data, design files and programs used for this study can be downloaded from Figshare (https://doi.org/10.6084/m9.figshare.14444672.v1) and Github (https://github.com/nkinar/WaterWatcher). The software is licensed using the GNU GPL v3 (https://www.gnu.org/licenses/gpl-3.0.en.html).

Authors' contributions

Both authors (N.K. and M.B.) contributed equally to this paper.

Ethics approval

Ethics approval is not applicable for this study.

Consent to participate

Consent to participate is not applicable for this study.

Consent for publication

Both authors consented to the publication of this manuscript.

612 **References**
613

614 Badamasi, Y. A. (2014). The working principle of an Arduino. In *2014 11th International Conference on*
615 *Electronics, Computer and Computation (ICECCO)* (pp. 1–4). Presented at the 2014 11th
616 International Conference on Electronics, Computer and Computation (ICECCO).
617 https://doi.org/10.1109/ICECCO.2014.6997578
618 Bassett, L. (2015). *Introduction to JavaScript Object Notation: A To-the-Point Guide to JSON*. California,
619 USA: O'Reilly Media, Inc.
620 Boehm, B., & Abts, C. (1999). COTS integration: plug and pray? *Computer*, *32*(1), 135–138. Presented at
621 the Computer. https://doi.org/10.1109/2.738311
622 Bonaccorsi, A., & Rossi, C. (2003). Why Open Source software can succeed. *Research Policy*, *32*(7), 1243–
623 1258. https://doi.org/10.1016/S0048-7333(03)00051-9
624 Borne, K. E. (2014). Floating treatment wetland influences on the fate and removal performance of
625 phosphorus in stormwater retention ponds. *Ecological Engineering*, *69*, 76–82.
626 https://doi.org/10.1016/j.ecoleng.2014.03.062
627 Brabec, E., Schulte, S., & Richards, P. L. (2002). Impervious Surfaces and Water Quality: A Review of
628 Current Literature and Its Implications for Watershed Planning. *Journal of Planning Literature*,
629 *16*(4), 499–514. https://doi.org/10.1177/088541202400903563
630 Chandrappa, S., Dharmanna, L., Bhatta UV, S. S., Sudeeksha, M., Suraksha, M. N., & Thrupthi, S. (2017).
631 Design and Development of IoT Device to Measure Quality of Water. *International Journal of*
632 *Modern Education and Computer Science*, *9*(4), 50–56.
633 https://doi.org/10.5815/ijmecs.2017.04.06
634 Chen, Y., & Han, D. (2018). Water quality monitoring in smart city: A pilot project. *Automation in*
635 *Construction*, *89*, 307–316. https://doi.org/10.1016/j.autcon.2018.02.008

636 Chowdury, M. S. U., Emran, T. B., Ghosh, S., Pathak, A., Alam, Mohd. M., Absar, N., et al. (2019). IoT
637 Based Real-time River Water Quality Monitoring System. *Procedia Computer Science*, *155*, 161–
638 168. https://doi.org/10.1016/j.procs.2019.08.025
639 Conley, D. J., Paerl, H. W., Howarth, R. W., Boesch, D. F., Seitzinger, S. P., Havens, K. E., et al. (2009).
640 Controlling Eutrophication: Nitrogen and Phosphorus. *Science*, *323*(5917), 1014–1015.
641 https://doi.org/10.1126/science.1167755
642 Das, B., & Jain, P. C. (2017). Real-time water quality monitoring system using Internet of Things. In *2017*
643 *International Conference on Computer, Communications and Electronics (Comptelix)* (pp. 78–82).
644 Presented at the 2017 International Conference on Computer, Communications and Electronics
645 (Comptelix). https://doi.org/10.1109/COMPTELIX.2017.8003942
646 Davies-Colley, R. J., & Smith, D. G. (2001). Turbidity Suspended Sediment, and Water Clarity: A Review.
647 *JAWRA Journal of the American Water Resources Association*, *37*(5), 1085–1101.
648 https://doi.org/10.1111/j.1752-1688.2001.tb03624.x
649 Deblonde, T., Cossu-Leguille, C., & Hartemann, P. (2011). Emerging pollutants in wastewater: A review of
650 the literature. *International Journal of Hygiene and Environmental Health*, *214*(6), 442–448.
651 https://doi.org/10.1016/j.ijheh.2011.08.002
652 DeFilippi, J. A., & Shih, C. S. (1971). Characteristics of Separated Storm and Combined Sewer Flows.
653 *Journal (Water Pollution Control Federation)*, *43*(10), 2033–2058.
654 Di Penta, M., German, D. M., Guéhéneuc, Y., & Antoniol, G. (2010). An exploratory study of the evolution
655 of software licensing. In *2010 ACM/IEEE 32nd International Conference on Software Engineering*
656 (Vol. 1, pp. 145–154). Presented at the 2010 ACM/IEEE 32nd International Conference on
657 Software Engineering. https://doi.org/10.1145/1806799.1806824
658 Dudak, J., Tanuska, P., Gaspar, G., & Fabo, P. (2018). ARM-Based Universal 1-Wire Module Solution.
659 *Journal of Sensors*, *2018*, 1–16. https://doi.org/10.1155/2018/5268247

660 Eisenreich, D., & DeMuth, B. (2003). *Designing Embedded Internet Devices*. Newnes.

661 Encinas, C., Ruiz, E., Cortez, J., & Espinoza, A. (2017). Design and implementation of a distributed IoT
662 system for the monitoring of water quality in aquaculture. In *2017 Wireless Telecommunications*
663 *Symposium (WTS)* (pp. 1–7). Presented at the 2017 Wireless Telecommunications Symposium
664 (WTS). https://doi.org/10.1109/WTS.2017.7943540

665 Farrell, C., Hassard, F., Jefferson, B., Leziart, T., Nocker, A., & Jarvis, P. (2018). Turbidity composition and
666 the relationship with microbial attachment and UV inactivation efficacy. *Science of The Total*
667 *Environment*, *624*, 638–647. https://doi.org/10.1016/j.scitotenv.2017.12.173

668 Fisher, D. K., & Gould, P. J. (2012). Open-Source Hardware Is a Low-Cost Alternative for Scientific
669 Instrumentation and Research. *Modern Instrumentation*, *01*(02), 8–20.
670 https://doi.org/10.4236/mi.2012.12002

671 Fitzgerald, B. (2006). The Transformation of Open Source Software. *MIS Quarterly*, *30*(3), 587–598.
672 https://doi.org/10.2307/25148740

673 García, E., Quiles, E., Correcher, A., & Morant, F. (2018). Sensor Buoy System for Monitoring Renewable
674 Marine Energy Resources. *Sensors*, *18*(4), 945. https://doi.org/10.3390/s18040945

675 Geetha, S., & Gouthami, S. (2017). Internet of things enabled real time water quality monitoring system.
676 *Smart Water*, *2*(1), 1. https://doi.org/10.1186/s40713-017-0005-y

677 Gholizadeh, M., Melesse, A., & Reddi, L. (2016). A Comprehensive Review on Water Quality Parameters
678 Estimation Using Remote Sensing Techniques. *Sensors*, *16*(8), 1298.
679 https://doi.org/10.3390/s16081298

680 Gleeson, T., Wang-Erlandsson, L., Zipper, S. C., Porkka, M., Jaramillo, F., Gerten, D., et al. (2020). The
681 Water Planetary Boundary: Interrogation and Revision. *One Earth*, *2*(3), 223–234.
682 https://doi.org/10.1016/j.oneear.2020.02.009

683 Goovaerts, P. (1997). *Geostatistics for Natural Resources Evaluation*. New York: Oxford University Press.

684 Gopavanitha, K., & Nagaraju, S. (2017). A low cost system for real time water quality monitoring and
685 controlling using IoT. In *2017 International Conference on Energy, Communication, Data*
686 *Analytics and Soft Computing (ICECDS)* (pp. 3227–3229). Presented at the 2017 International
687 Conference on Energy, Communication, Data Analytics and Soft Computing (ICECDS).
688 https://doi.org/10.1109/ICECDS.2017.8390054
689 Haslett, J. (1997). On the sample variogram and the sample autocovariance for non-stationary time
690 series. *Journal of the Royal Statistical Society: Series D (The Statistician)*, *46*(4), 475–484.
691 https://doi.org/10.1111/1467-9884.00101
692 Henley, W. F., Patterson, M. A., Neves, R. J., & Lemly, A. D. (2000). Effects of Sedimentation and
693 Turbidity on Lotic Food Webs: A Concise Review for Natural Resource Managers. *Reviews in*
694 *Fisheries Science*, *8*(2), 125–139. https://doi.org/10.1080/10641260091129198
695 Ivan, I. A., Stihi, V., Ivan, M., Stihi, C., Rokotondrabe, M., & Jelea, A. (2011). Battery powered cost
696 effective TDS logger intended for water testing. *Romanian Journal of Physics*, *56*, 540–549.
697 Kamaludin, K. H., & Ismail, W. (2017). Water quality monitoring with internet of things (IoT). In *2017 IEEE*
698 *Conference on Systems, Process and Control (ICSPC)* (pp. 18–23). Presented at the 2017 IEEE
699 Conference on Systems, Process and Control (ICSPC).
700 https://doi.org/10.1109/SPC.2017.8313015
701 Karr, J. R., & Dudley, D. R. (1981). Ecological perspective on water quality goals. *Environmental*
702 *Management*, *5*(1), 55–68. https://doi.org/10.1007/BF01866609
703 Lee, M., Hwang, J., & Yoe, H. (2013). Agricultural Production System Based on IoT. In *2013 IEEE 16th*
704 *International Conference on Computational Science and Engineering* (pp. 833–837). Presented at
705 the 2013 IEEE 16th International Conference on Computational Science and Engineering.
706 https://doi.org/10.1109/CSE.2013.126

Li, L., Xiaoguang, H., Ke, C., & Ketai, H. (2011). The applications of WiFi-based Wireless Sensor Network in Internet of Things and Smart Grid. In *2011 6th IEEE Conference on Industrial Electronics and Applications* (pp. 789–793). Presented at the 2011 6th IEEE Conference on Industrial Electronics and Applications. https://doi.org/10.1109/ICIEA.2011.5975693

Li, T., Xia, M., Chen, J., Zhao, Y., & De Silva, C. (2017). Automated Water Quality Survey and Evaluation Using an IoT Platform with Mobile Sensor Nodes. *Sensors*, *17*(8), 1735. https://doi.org/10.3390/s17081735

Liu, J., & Hekkenberg, R. (2017). Sixty years of research on ship rudders: effects of design choices on rudder performance. *Ships and Offshore Structures*, *12*(4), 495–512. https://doi.org/10.1080/17445302.2016.1178205

Madrid, Y., & Zayas, Z. P. (2007). Water sampling: Traditional methods and new approaches in water sampling strategy. *TrAC Trends in Analytical Chemistry*, *26*(4), 293–299. https://doi.org/10.1016/j.trac.2007.01.002

Mangalvedhe, N., Ratasuk, R., & Ghosh, A. (2016). NB-IoT deployment study for low power wide area cellular IoT. In *2016 IEEE 27th Annual International Symposium on Personal, Indoor, and Mobile Radio Communications (PIMRC)* (pp. 1–6). Presented at the 2016 IEEE 27th Annual International Symposium on Personal, Indoor, and Mobile Radio Communications (PIMRC). https://doi.org/10.1109/PIMRC.2016.7794567

Marsalek, J. (1991). Pollutant Loads in Urban Stormwater: Review of Methods for Planning-Level Estimates. *JAWRA Journal of the American Water Resources Association*, *27*(2), 283–291. https://doi.org/10.1111/j.1752-1688.1991.tb03133.x

McGrane, S. J. (2016). Impacts of urbanisation on hydrological and water quality dynamics, and urban water management: a review. *Hydrological Sciences Journal*, *61*(13), 2295–2311. https://doi.org/10.1080/02626667.2015.1128084

731 Moparthi, N. R., Mukesh, Ch., & Vidya Sagar, P. (2018). Water Quality Monitoring System Using IOT. In
732 *2018 Fourth International Conference on Advances in Electrical, Electronics, Information,*
733 *Communication and Bio-Informatics (AEEICB)* (pp. 1–5). Presented at the 2018 Fourth
734 International Conference on Advances in Electrical, Electronics, Information, Communication
735 and Bio-Informatics (AEEICB). https://doi.org/10.1109/AEEICB.2018.8480963
736 Myint, C. Z., Gopal, L., & Aung, Y. L. (2017). Reconfigurable smart water quality monitoring system in IoT
737 environment. In *2017 IEEE/ACIS 16th International Conference on Computer and Information*
738 *Science (ICIS)* (pp. 435–440). Presented at the 2017 IEEE/ACIS 16th International Conference on
739 Computer and Information Science (ICIS). https://doi.org/10.1109/ICIS.2017.7960032
740 Nadaf, R., & Bonal, V. (2019). Smart Mirror using Raspberry Pi as a Security and Vigilance System. In
741 *2019 3rd International Conference on Trends in Electronics and Informatics (ICOEI)* (pp. 360–
742 365). Presented at the 2019 3rd International Conference on Trends in Electronics and
743 Informatics (ICOEI). https://doi.org/10.1109/ICOEI.2019.8862537
744 Ng, I. C. L., & Wakenshaw, S. Y. L. (2017). The Internet-of-Things: Review and research directions.
745 *International Journal of Research in Marketing*, *34*(1), 3–21.
746 https://doi.org/10.1016/j.ijresmar.2016.11.003
747 Oropallo, W., & Piegl, L. A. (2016). Ten challenges in 3D printing. *Engineering with Computers*, *32*(1),
748 135–148. https://doi.org/10.1007/s00366-015-0407-0
749 Pal, A., Rath, H. K., Shailendra, S., & Bhattacharyya, A. (2018). IoT Standardization: The Road Ahead. In J.
750 Sen (Ed.), *Internet of Things - Technology, Applications and Standardization*. InTech.
751 https://doi.org/10.5772/intechopen.75137
752 Parameswari, M., & Moses, M. B. (2019). Efficient analysis of water quality measurement reporting
753 system using IOT based system in WSN. *Cluster Computing*, *22*(5), 12193–12201.
754 https://doi.org/10.1007/s10586-017-1581-1

Pasika, S., & Gandla, S. T. (2020). Smart water quality monitoring system with cost-effective using IoT. *Heliyon*, *6*(7), e04096. https://doi.org/10.1016/j.heliyon.2020.e04096

Paul, M. J., Coffey, R., Stamp, J., & Johnson, T. (2019). A Review of Water Quality Responses to Air Temperature and Precipitation Changes 1: Flow, Water Temperature, Saltwater Intrusion. *JAWRA Journal of the American Water Resources Association*, *55*(4), 824–843. https://doi.org/10.1111/1752-1688.12710

Pearce, J. M. (2012). Building Research Equipment with Free, Open-Source Hardware. *Science*, *337*(6100), 1303–1304. https://doi.org/10.1126/science.1228183

Pranata, A. A., Jae Min Lee, & Dong Seong Kim. (2017). Towards an IoT-based water quality monitoring system with brokerless pub/sub architecture. In *2017 IEEE International Symposium on Local and Metropolitan Area Networks (LANMAN)* (pp. 1–6). Presented at the 2017 IEEE International Symposium on Local and Metropolitan Area Networks (LANMAN). https://doi.org/10.1109/LANMAN.2017.7972166

Prasad, A. N., Mamun, K. A., Islam, F. R., & Haqva, H. (2015). Smart water quality monitoring system. In *2015 2nd Asia-Pacific World Congress on Computer Science and Engineering (APWC on CSE)* (pp. 1–6). Presented at the 2015 2nd Asia-Pacific World Congress on Computer Science and Engineering (APWC on CSE). https://doi.org/10.1109/APWCCSE.2015.7476234

Prathibha, S. R., Hongal, A., & Jyothi, M. P. (2017). IOT Based Monitoring System in Smart Agriculture. In *2017 International Conference on Recent Advances in Electronics and Communication Technology (ICRAECT)* (pp. 81–84). Presented at the 2017 International Conference on Recent Advances in Electronics and Communication Technology (ICRAECT). https://doi.org/10.1109/ICRAECT.2017.52

Raju, K. R. S. R., & Varma, G. H. K. (2017). Knowledge Based Real Time Monitoring System for Aquaculture Using IoT. In *2017 IEEE 7th International Advance Computing Conference (IACC)* (pp.

318–321). Presented at the 2017 IEEE 7th International Advance Computing Conference (IACC). https://doi.org/10.1109/IACC.2017.0075

Rusydi, A. F. (2018). Correlation between conductivity and total dissolved solid in various type of water: A review. *IOP Conference Series: Earth and Environmental Science*, *118*, 012019. https://doi.org/10.1088/1755-1315/118/1/012019

Salerno, D., & Korsunsky, R. (1998). Practical considerations in the design of lithium-ion battery protection systems. In *APEC'98 Thirteenth Annual Applied Power Electronics Conference and Exposition* (Vol. 2, pp. 700–707 vol.2). Presented at the APEC '98 Thirteenth Annual Applied Power Electronics Conference and Exposition. https://doi.org/10.1109/APEC.1998.653975

Saravanan, K., Anusuya, E., Kumar, R., & Son, L. H. (2018). Real-time water quality monitoring using Internet of Things in SCADA. *Environmental Monitoring and Assessment*, *190*(9), 556. https://doi.org/10.1007/s10661-018-6914-x

Saravanan, M., Das, A., & Iyer, V. (2017). Smart water grid management using LPWAN IoT technology. In *2017 Global Internet of Things Summit (GIoTS)* (pp. 1–6). Presented at the 2017 Global Internet of Things Summit (GIoTS). https://doi.org/10.1109/GIOTS.2017.8016224

Sarik, J., & Kymissis, I. (2010). Lab kits using the Arduino prototyping platform. In *2010 IEEE Frontiers in Education Conference (FIE)* (pp. T3C-1-T3C-5). Presented at the 2010 IEEE Frontiers in Education Conference (FIE). https://doi.org/10.1109/FIE.2010.5673417

Shen, R., Honghao, Y., Noble, B., Zeng, W., Gersher, S., Phung, T., et al. (2019). A GIS-based model of ecosystem services for the Northeast Swale in Saskatoon, Saskatchewan. *Spatial Knowledge and Information Canada*, *7*(1), 4.

Suo, H., Wan, J., Zou, C., & Liu, J. (2012). Security in the Internet of Things: A Review. In *2012 International Conference on Computer Science and Electronics Engineering* (Vol. 3, pp. 648–651).

802 Presented at the 2012 International Conference on Computer Science and Electronics
803 Engineering. https://doi.org/10.1109/ICCSEE.2012.373
804 Terada, D., Tamashima, M., Nakao, I., & Matsuda, A. (2019). Estimation of metacentric height using
805 onboard monitoring roll data based on time series analysis. *Journal of Marine Science and*
806 *Technology*, *24*(1), 285–296. https://doi.org/10.1007/s00773-018-0552-4
807 Texas Instruments. (2011). *Evaluation Board / Kit Important Notice (ssyz019j)*. Dallas: Texas Instruments.
808 https://www.ti.com/lit/pdf/ssyz019
809 Vijayakumar, N., & Ramya, R. (2015). The real time monitoring of water quality in IoT environment. In
810 *2015 International Conference on Innovations in Information, Embedded and Communication*
811 *Systems (ICIIECS)* (pp. 1–5). Presented at the 2015 International Conference on Innovations in
812 Information, Embedded and Communication Systems (ICIIECS).
813 https://doi.org/10.1109/ICIIECS.2015.7193080
814 Vlaming, V. de, Connor, V., DiGiorgio, C., Bailey, H. C., Deanovic, L. A., & Hinton, D. E. (2000). Application
815 of whole effluent toxicity test procedures to ambient water quality assessment. *Environmental*
816 *Toxicology and Chemistry*, *19*(1), 42–62. https://doi.org/10.1002/etc.5620190106
817 Weber-Scan, P. K., & Duffy, L. K. (2007). Effects of Total Dissolved Solids on Aquatic Organisms: A Review
818 of Literature and Recommendation for Salmonid Species. *American Journal of Environmental*
819 *Sciences*, *3*(1), 1–6. https://doi.org/10.3844/ajessp.2007.1.6
820 Willocx, M., Bohé, I., Vossaert, J., & Naessens, V. (2018). Developing Maintainable Application-Centric
821 IoT Ecosystems. In *2018 IEEE International Congress on Internet of Things (ICIOT)* (pp. 25–32).
822 Presented at the 2018 IEEE International Congress on Internet of Things (ICIOT).
823 https://doi.org/10.1109/ICIOT.2018.00011

824 Wong, B. P., & Kerkez, B. (2016). Real-time environmental sensor data: An application to water quality
825 using web services. *Environmental Modelling & Software*, *84*, 505–517.
826 https://doi.org/10.1016/j.envsoft.2016.07.020
827 Yu, L., Kin-Fai, T., Xiangdong, Q., Ying, L., & Xuyang, D. (2017). Wireless Mesh Networks in IoT networks.
828 In *2017 International Workshop on Electromagnetics: Applications and Student Innovation*
829 *Competition* (pp. 183–185). Presented at the 2017 International Workshop on Electromagnetics:
830 Applications and Student Innovation Competition. https://doi.org/10.1109/iWEM.2017.7968828
831 Zumbahlenas, H. (Ed.). (2008). *Linear circuit design handbook*. Amsterdam ; Boston: Elsevier/Newnes
832 Press.

833
834
835 **Appendices**
836
837 Appendix A and B are provided as PDF files as Supplementary Information (SI).

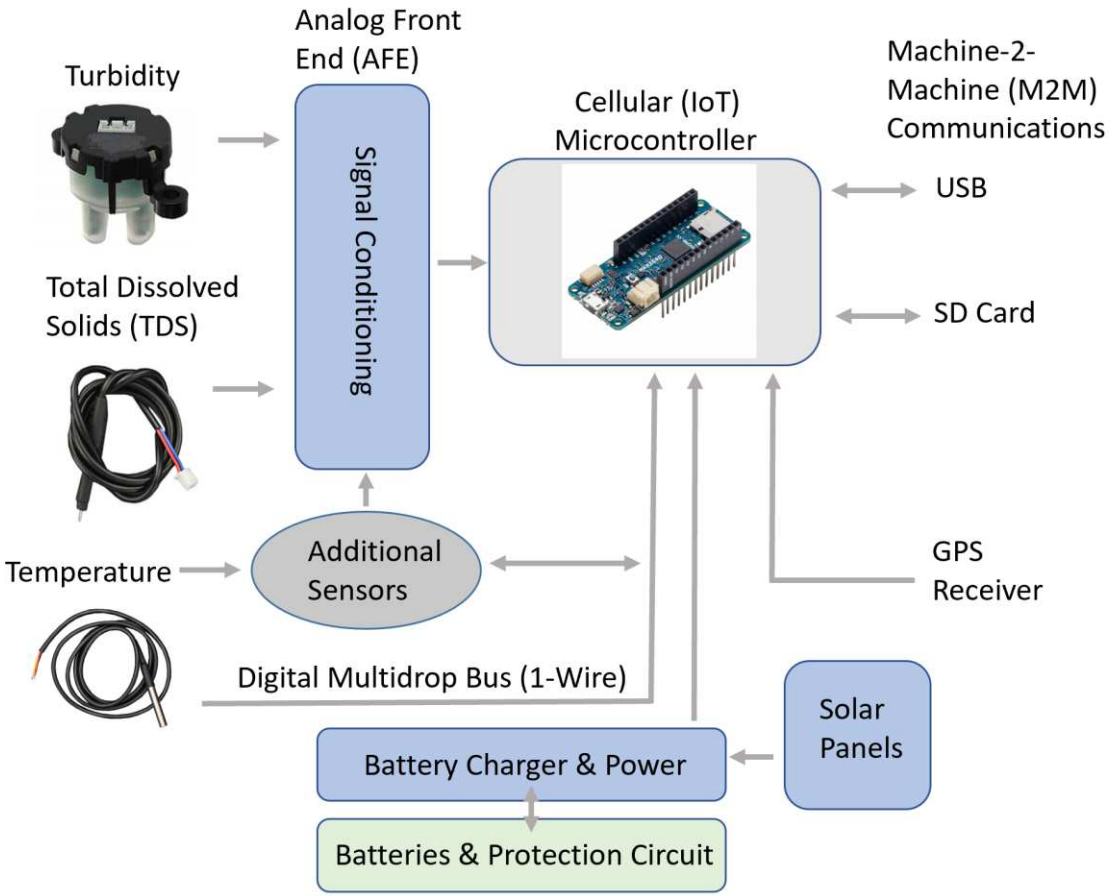

Figure 1. Block diagram of WaterWatcher system showing sub-systems. Photographs courtesy Digikey Incorporated (Thief River Falls, Minnesota, USA) and are used with permission.

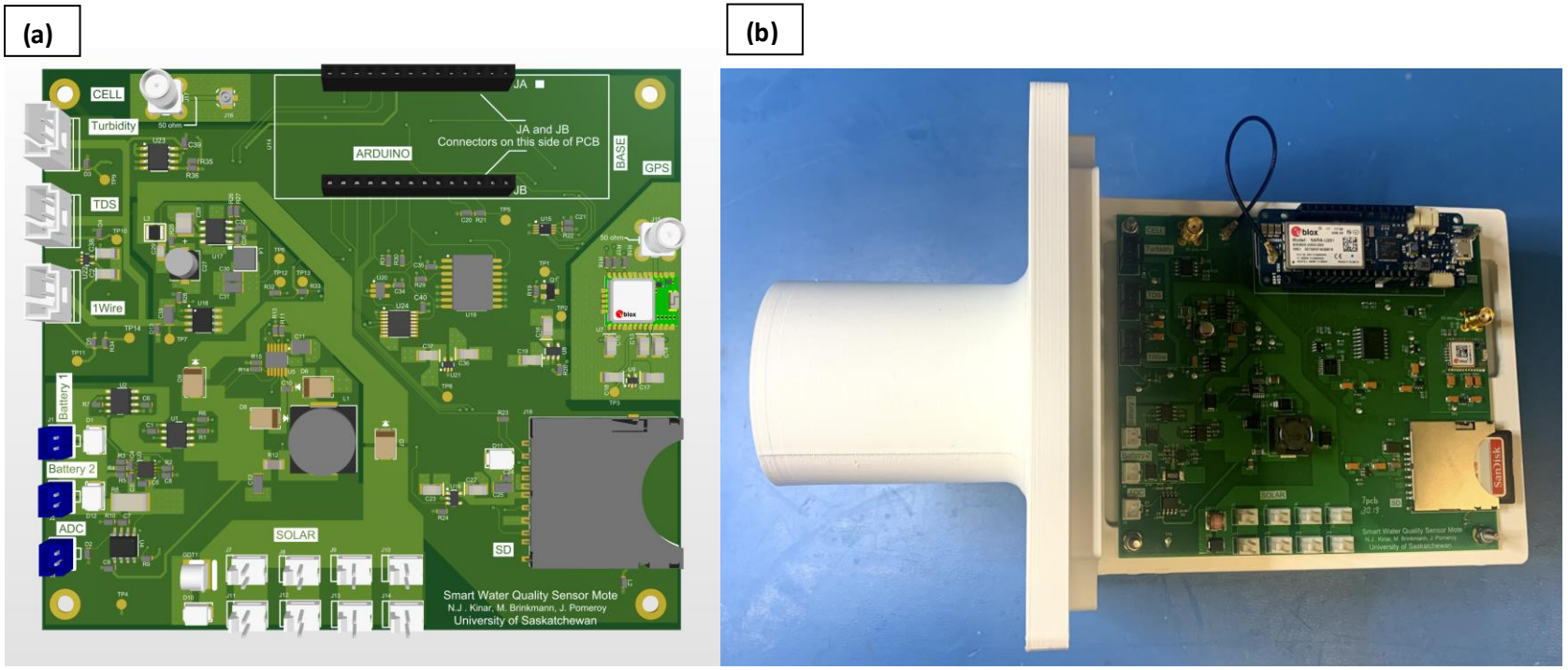

Figure 2. (a) 3D rendering of the electronic printed circuit board (PCB) for the WaterWatcher system. System components are labeled on the PCB. (b) Picture of constructed PCB mounted with mechanical fasteners on a 3D printed plastic part.

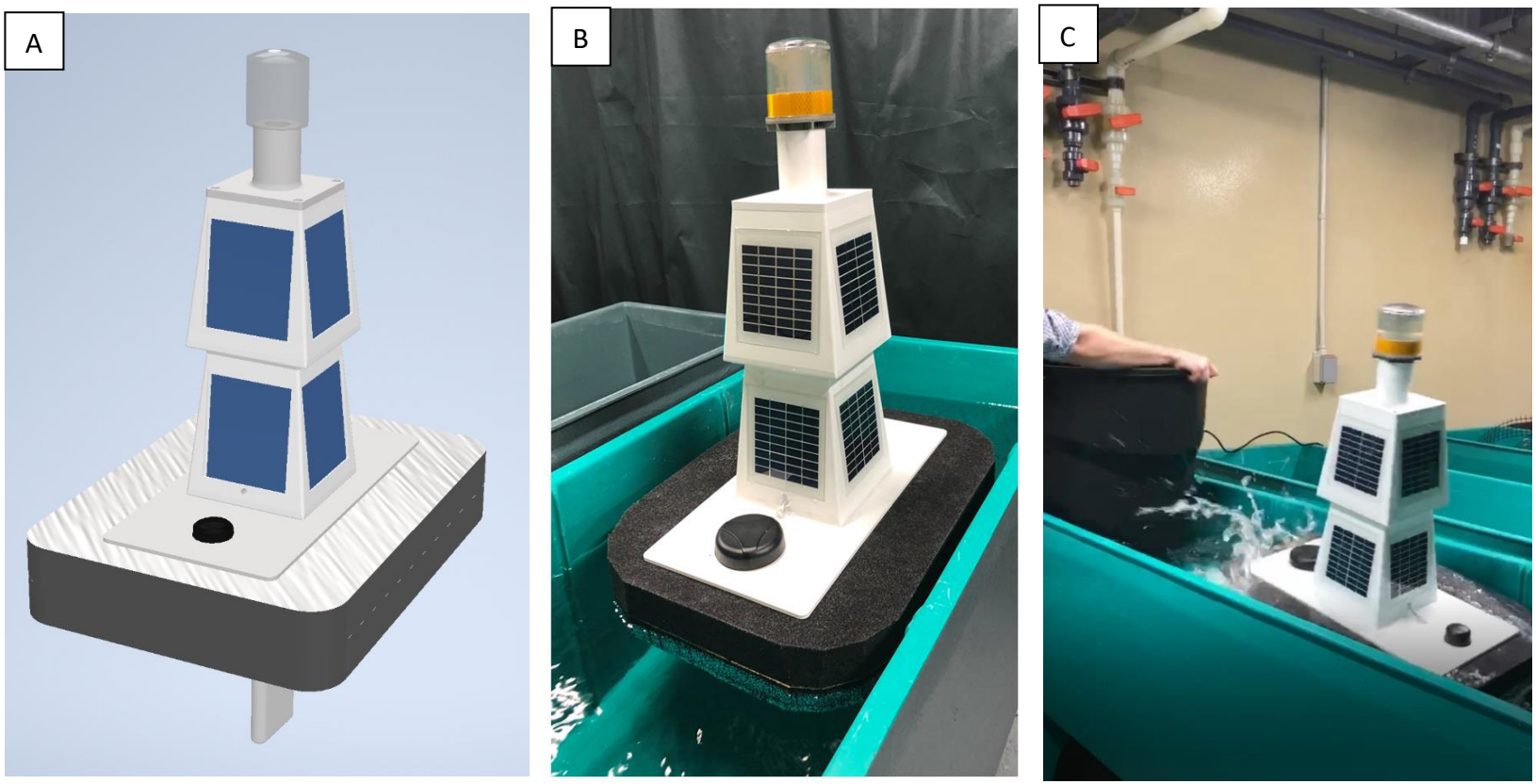

Figure 3. (a) CAD software rendering of mechanical WaterWatcher enclosure. The 3D model includes all mechanical parts that comprise the system. (b) Actual photograph of the WaterWatcher system tested in a tank. (c) Photograph of tank test to check for buoyancy and stability.

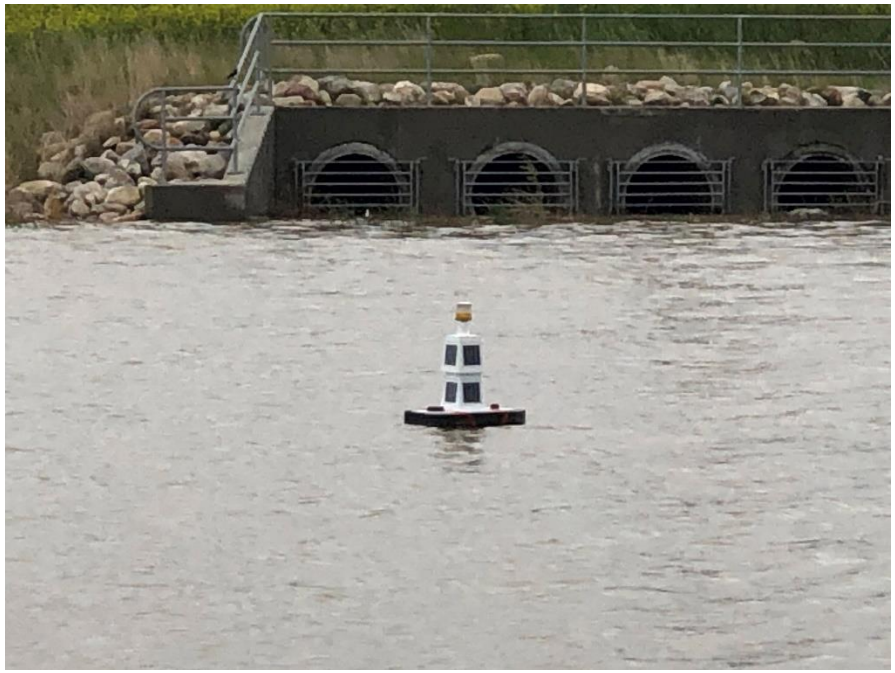

Figure 4. Deployment of WaterWatcher at an urban reservoir (Aspen Ridge Forebay, City of Saskatoon, Saskatoon, Saskatchewan, Canada).

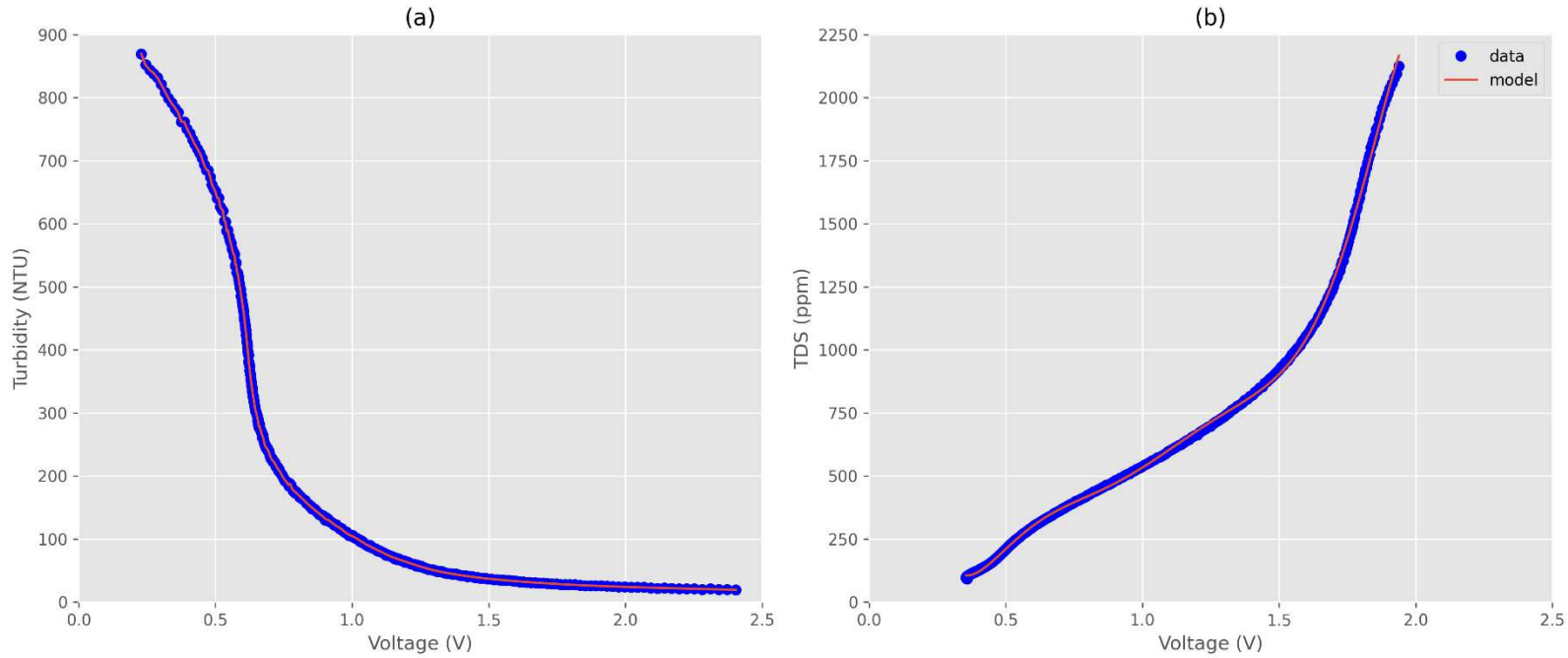

Figure 5. Calibration experiments to relate sensor output voltages to (a) turbidity and (b) TDS. The data are shown as circle markers, whereas the model is shown as a line on each plot.

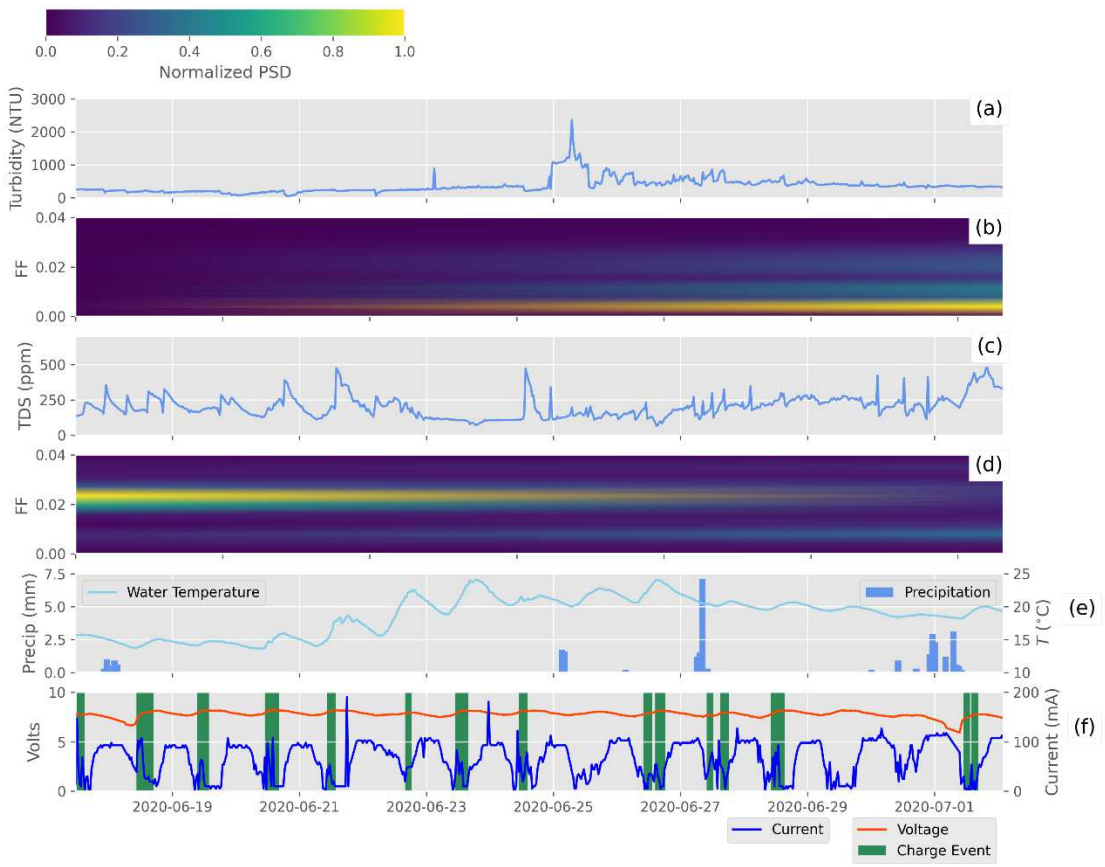

Figure 6. Field data collected at the Aspen Ridge Forebay location. (a) Turbidity time series; (b) spectrogram of turbidity time series with fractional frequency (FF); (c) TDS time series; (d) spectrogram of TDS time series with fractional frequency (FF); (e) precipitation events as measured at Saskatoon by Environment and Climate Change Canada along with reservoir water temperature $T\ (^{\circ}\mathrm{C})$; (f) time series of battery voltage showing discrete battery charging events associated with operation of the solar panel battery charger and battery current consumption. As shown by the colorbar at the top of the figure, the spectrogram Power Spectral Density (PSD) has been normalized with respect to the maximum power of the time series signals associated with spectrograms (b) and (d).

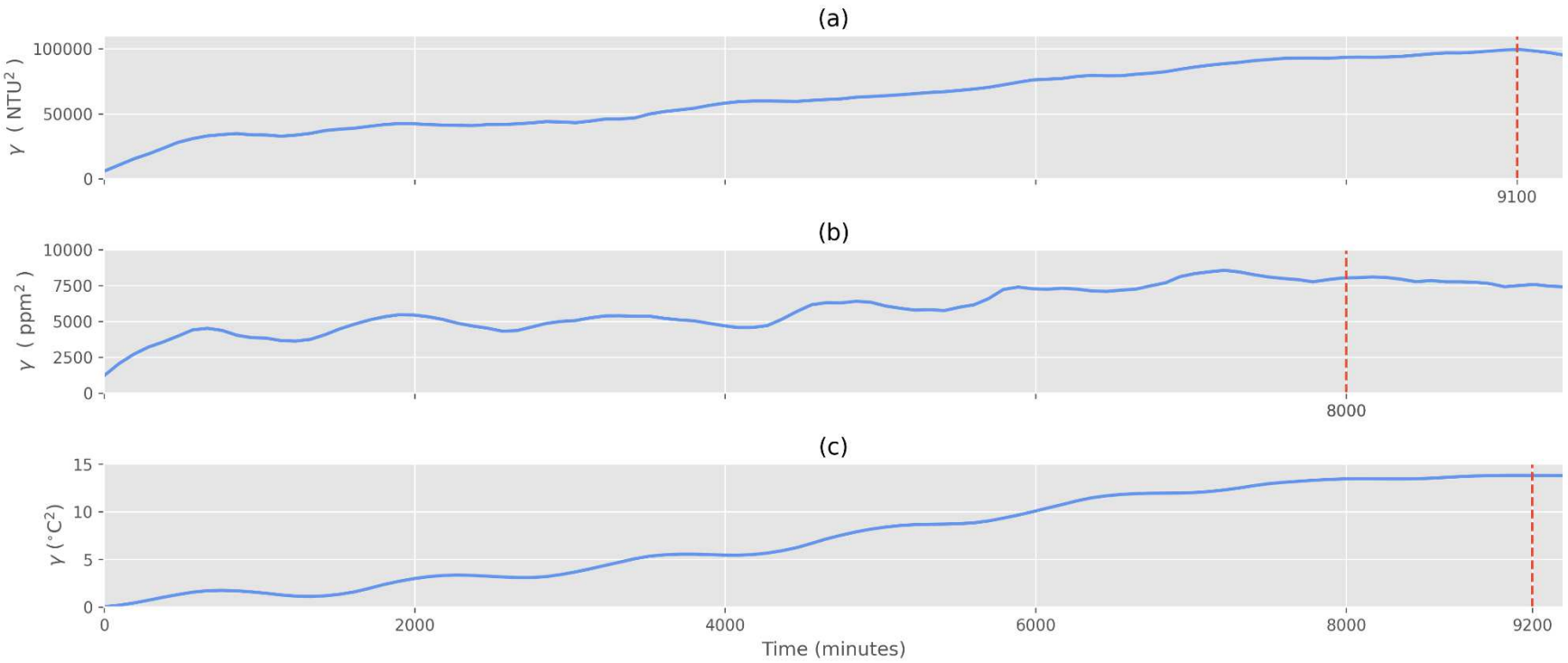

Figure 7. Semivariance γ of (a) turbidity, (b) TDS and (c) water temperature time series. The range is marked on the x-axis as a vertical dashed line to indicate temporal autocorrelation at time intervals less than the range.

Table 1. Arduino setup code for WaterWatcher platform showing how system functionality is encapsulated by a WaterWatcher object. Some other functionality is provided by the CLI (Table 2), thereby reducing the amount of code required to be written by the user. The *Arduino.h* header file is only to be included when using an alternate IDE such as provided by Platform.io and is not required for the official Arduino IDE.

```
#include <Arduino.h>
#include <WaterWatcher.h>
#include "WaterWatcherOptions.h"

class MyWaterWatcherOptions : public WaterWatcherOptions
{
    public:

        MyWaterWatcherOptions()
        {
            sample_a0(true);        // sample a0
            sample_a1(true);        // sample a1
            sample_a2(false);       // do not sample a2
            sample_temp0(true);     // sample temp0
        } // end

        //-------------------------------------------------
        // TRANSFER FUNCTION OUTPUTS
        // EDIT THESE FUNCTIONS IF REQUIRED
        //-------------------------------------------------
        float get_a0_out()
        {
            float out = get_a0_raw();
            return out;
        } // end

        float get_a1_out()
        {
            float out = get_a1_raw();
            return out;
        } // end

        float get_a2_out()
        {
            float out = get_a2_raw();
            return out;
        } // end

        float get_temp0_out()
        {
            float out = get_temp0_raw();
            return out;
        } // end

}; // end

// Create an instance of the WaterWatcher object
WaterWatcher ww;

// Create an instance of the options object
MyWaterWatcherOptions opt;

// Required Arduino setup function
```

```
54. void setup()
55. {
56.   ww.setup(&opt);
57. } // end
58.
59. // Required Arduino main loop
60. void loop()
61. {
62.   ww.checkState();
63. } // end
```

Table 2. Commands for the Command Line Interface (CLI) listed along with examples. The CLI controls the state machine implemented in software and allows for system functionality to be set. Example functionality of commands are also given in the table. After the sampling rate is set, the write-flash command should be used to save the state into non-volatile memory. As demonstrated by the commands, the CLI allows for system functionality to be easily configured.

Software Commands	
on-5v	Turn on 5V power on circuit board
off-5v	Turn off 5V power on circuit board
print-serial	Print serial number
bstate	Print battery state
rtemp	RTC clock temperature
time	Print the current time
time dd/mm/yyyy hh:mm:ss	Set the current time (24 hour clock)
rtc-control	Read the status of the RTC control register
rtc-default	Set the RTC to defaults
sam [n]	Set alarm every n minutes (alarm is on after command)
oa	Turn off alarm
iao	Is alarm on?
print-coeff	Print flash coefficients
set-name [name]	Set the name of the device
write-flash	Write non-volatile vars into flash
read-flash	Read non-volatile vars
mem-defaults	Clear the memory to defaults
bmon-addr	Print the battery monitor addresses
print-bmon	Print the battery monitor information
reset	Reset the device (i.e. powercycle)
print-gps	Print the GPS coordinates
on-sd	Turn on the SD card
off-sd	Turn off the SD card
ls	List the contents of the SD card
cat [filename]	List the contents of a file on the SD card
rm [filename]	Remove a file from the card

echo [filename] [message]	Echo a message to file
key [number]	Set a key for communications with the server
cell [string]	Send a string over the cellular network to the server
on-cell	Turn on the cellular modem
off-cell	Turn off the cellular modem
powersave-on	Turn on powersave (i.e. shutdown modem and rails)
powersave-off	Turn off powersave
sendcell-on	Turn on sending of the cellular device
sendcell-off	Turn off sending of the cellular device
sample	Manually trigger a sample

Table 3. Calibration model accuracies for the WaterWatcher obtained from laboratory experimentation. The Root Mean Squared Difference (RMSD) is listed along with the Mean Bias (MB). The resolution is calculated as per the discussion in Section 3.1.

Measure	Turbidity (NTU)	TDS (ppm)
RMSD	1.0	11.38
MB	1.753e-13	-0.01348
Sensor Resolution	0.7454	1.007

Appendix A

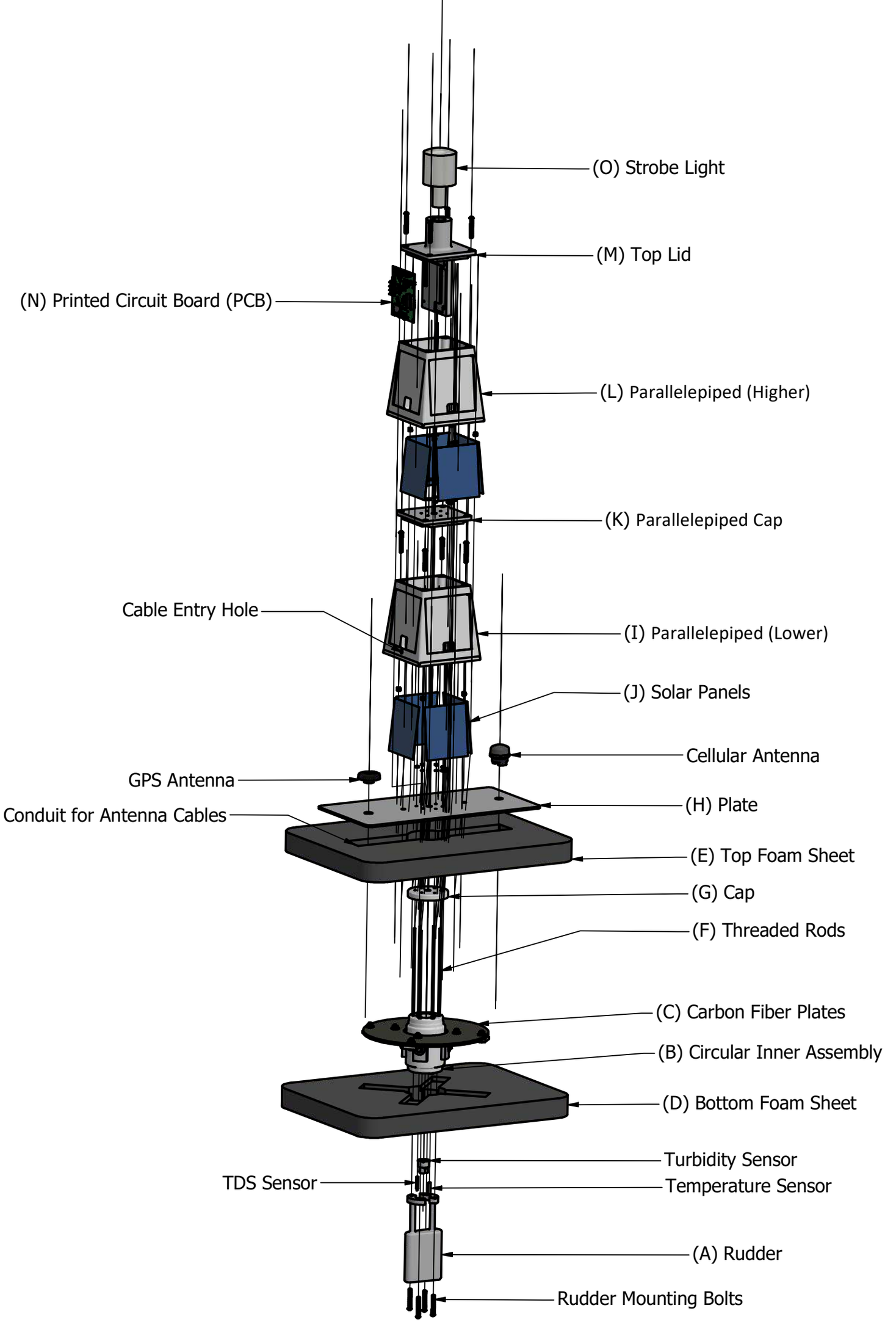
(O) Strobe Light
(M) Top Lid
(N) Printed Circuit Board (PCB)
(L) Parallelepiped (Higher)
(K) Parallelepiped Cap
Cable Entry Hole
(I) Parallelepiped (Lower)
(J) Solar Panels
Cellular Antenna
GPS Antenna
(H) Plate
Conduit for Antenna Cables
(E) Top Foam Sheet
(G) Cap
(F) Threaded Rods
(C) Carbon Fiber Plates
(B) Circular Inner Assembly
(D) Bottom Foam Sheet
Turbidity Sensor
TDS Sensor
Temperature Sensor
(A) Rudder
Rudder Mounting Bolts

Appendix B

Battery Protector / Charge Balancing / Fuel Gauge

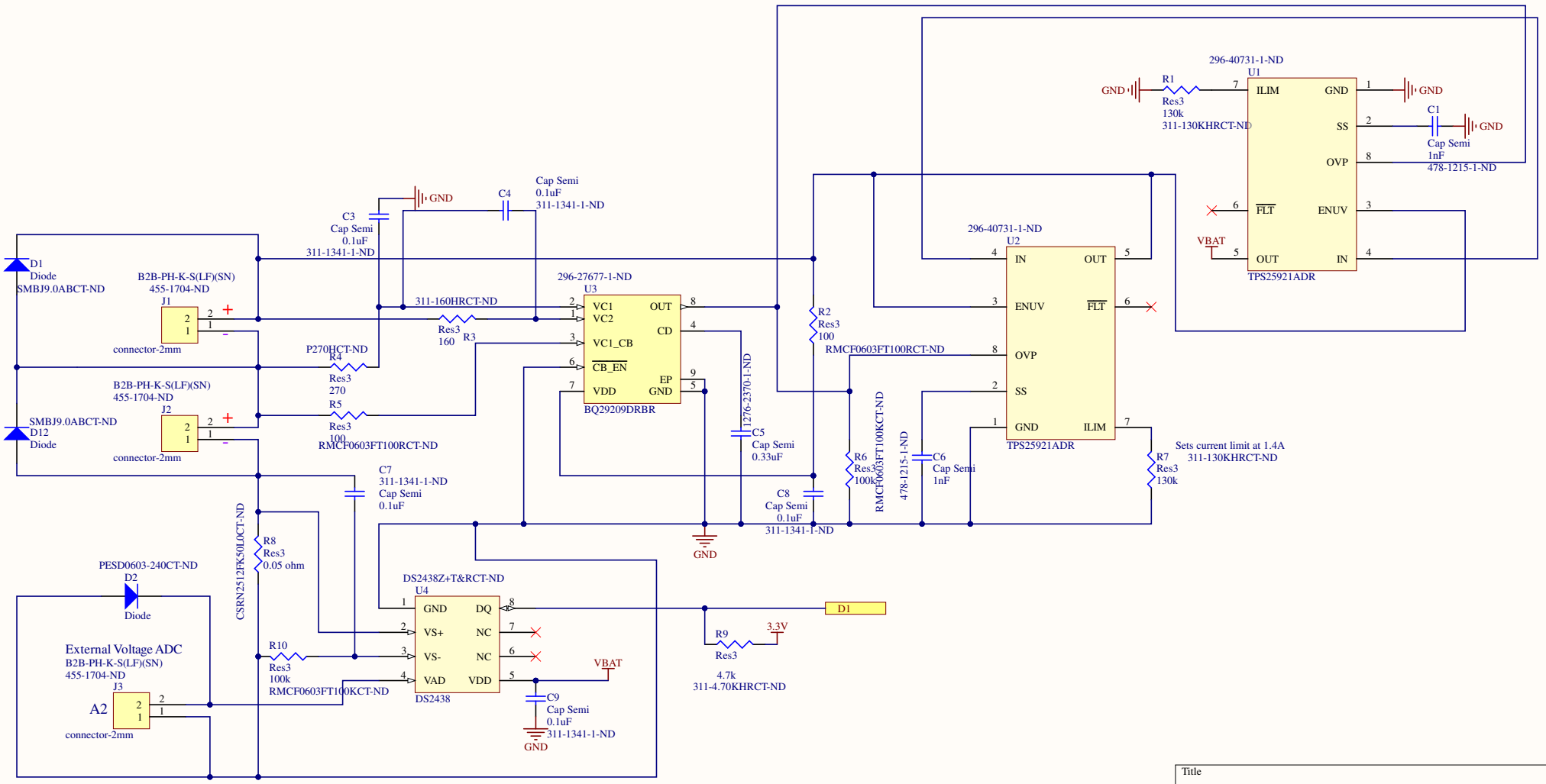

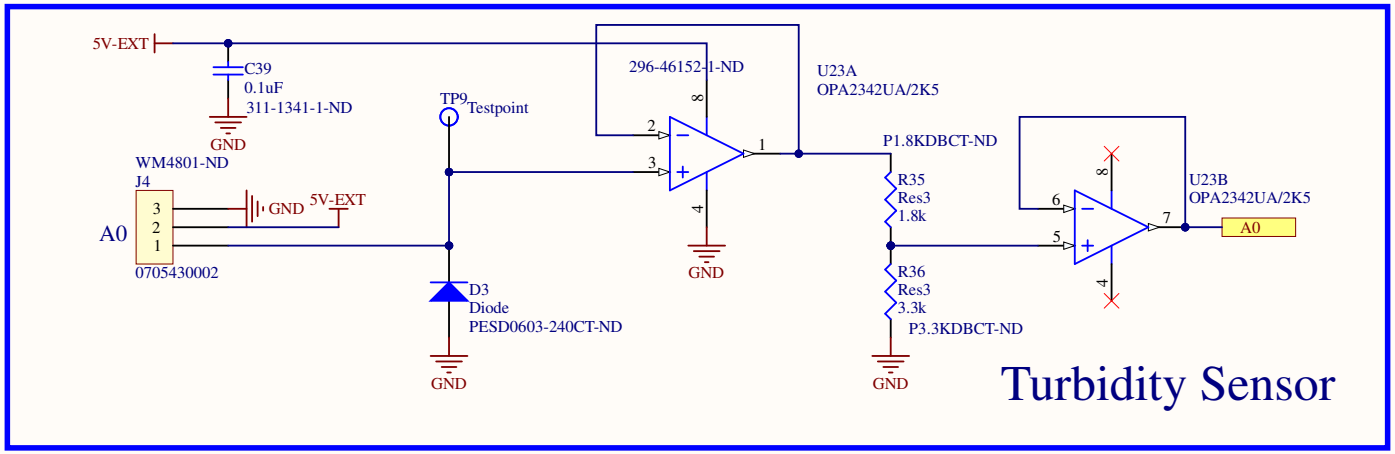

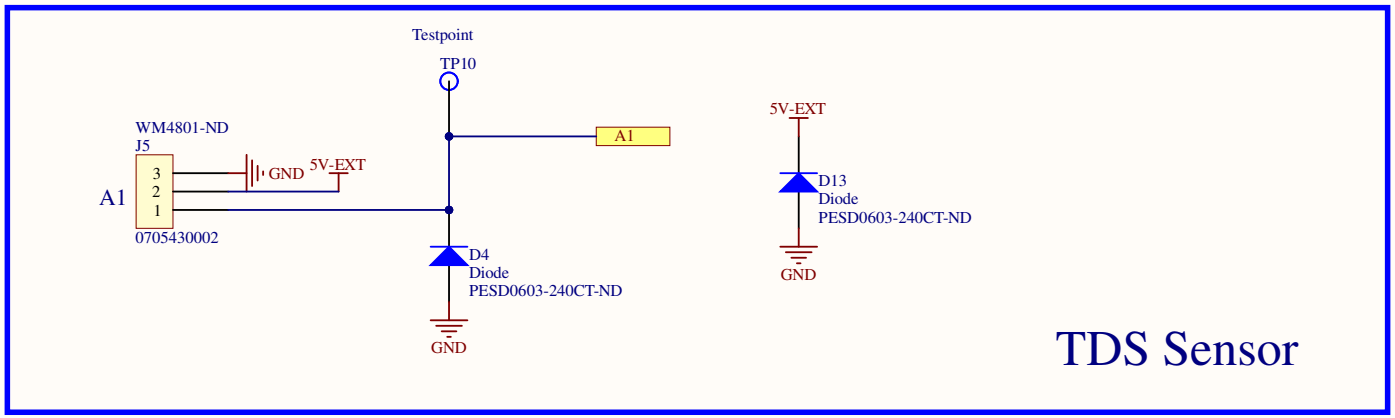

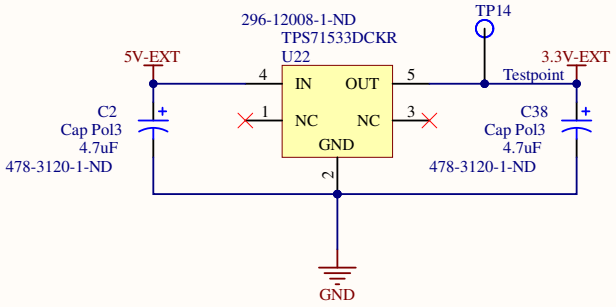

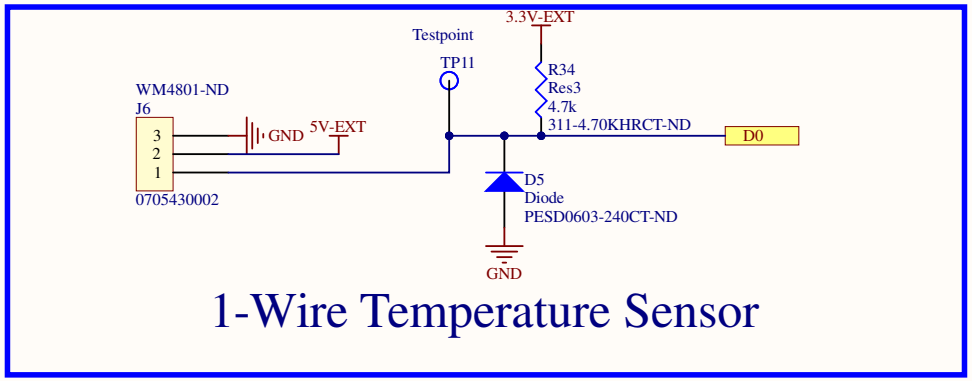

Title		
Size: Letter	Number	Revision
Date: 4-09-2021		Sheet of
File: K:\OneDrive\..\breakout-1.SchDoc		Drawn By:

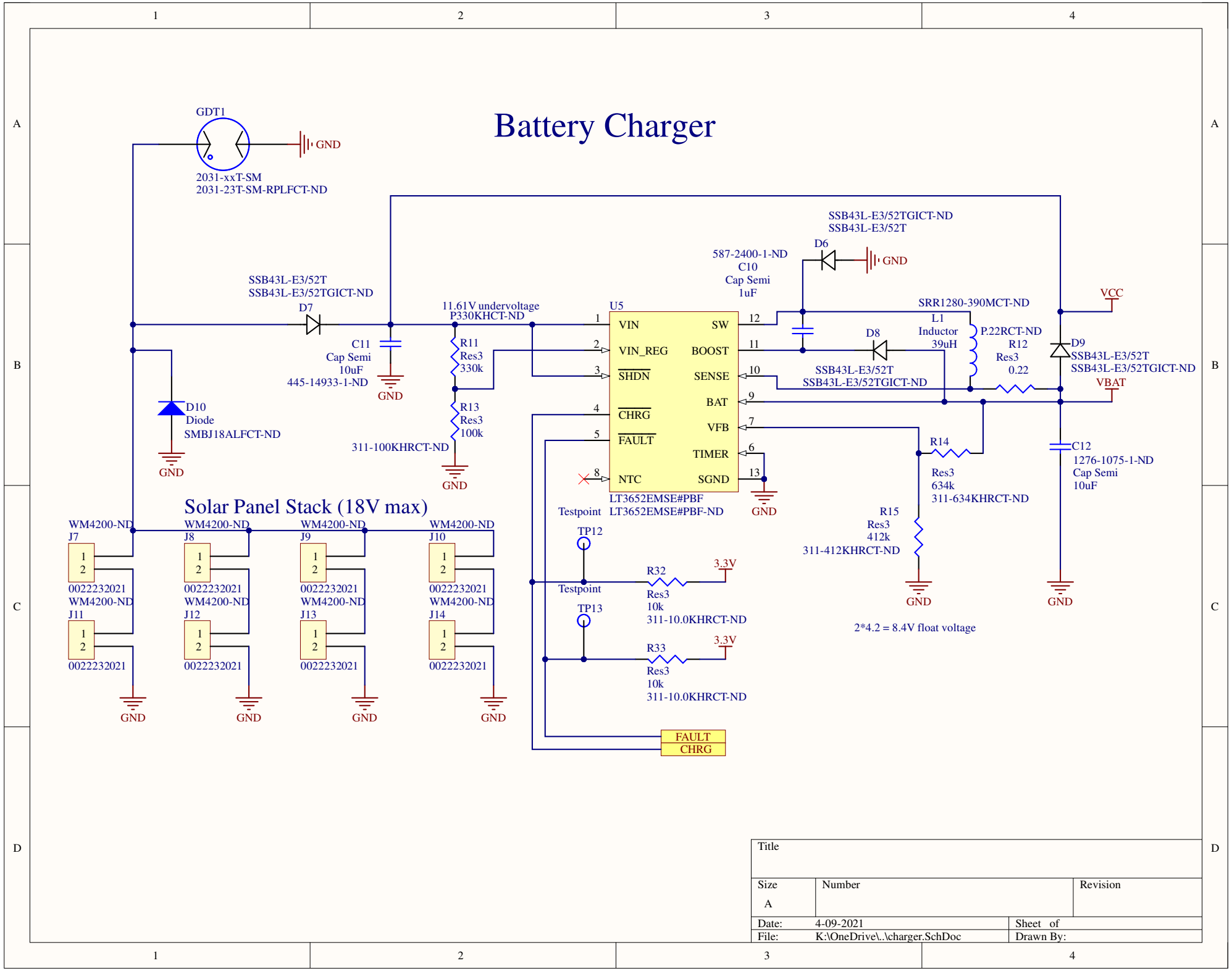
Battery Charger
GDT1
GND
2031-xxT-SM
2031-23T-SM-RPLFCT-ND
SSB43L-E3/52TGICT-ND
SSB43L-E3/52T
D6
587-2400-1-ND
C10
Cap Semi
1uF
SSB43L-E3/52T
SSB43L-E3/52TGICT-ND
D7
11.61V undervoltage
P330KHCT-ND
U5
VIN
VIN_REG
SHDN
CHRG
FAULT
NTC
SW
BOOST
SENSE
BAT
VFB
TIMER
SGND
LT3652EMSE#PBF
LT3652EMSE#PBF-ND
SRR1280-390MCT-ND
L1
Inductor
39uH
P.22RCT-ND
R12
Res3
0.22
D8
SSB43L-E3/52T
SSB43L-E3/52TGICT-ND
D9
SSB43L-E3/52T
SSB43L-E3/52TGICT-ND
VCC
VBAT
C11
Cap Semi
10uF
445-14933-1-ND
R11
Res3
330k
R13
Res3
100k
311-100KHRCT-ND
D10
Diode
SMBJ18ALFCT-ND
R14
Res3
634k
311-634KHRCT-ND
C12
1276-1075-1-ND
Cap Semi
10uF
R15
Res3
412k
311-412KHRCT-ND
Solar Panel Stack (18V max)
WM4200-ND
J7
J8
J9
J10
J11
J12
J13
J14
0022232021
Testpoint
TP12
TP13
R32
R33
Res3
10k
311-10.0KHRCT-ND
3.3V
2*4.2 = 8.4V float voltage
FAULT
CHRG
Title
Size
A
Number
Revision
Date:
4-09-2021
Sheet of
File:
K:\OneDrive\..\charger.SchDoc
Drawn By:

GPS

Control impedance of antenna trace with width 0.75 mm. Control impedance to 50 ohms. Starting trace width at 0.75 mm and trace gap at 0.15 mm with surrounding GND plane. Adjust trace width and gap accordingly to attain specified impedance.

A.80.A.101111
931-1528-ND
U6
Mechanical
*

An external bias tee is required for the RF antenna to work. On an updated version of the PCB, the bias tee should be present on the PCB.

CAM-M8
672-1013-1-ND
U7

A97594-ND
J15
5-1814832-1

R16 311-220HRCT-ND
Res3
220 ohm

R17 311-220HRCT-ND
Res3
220 ohm

R18 311-220HRCT-ND
Res3
220 ohm

TX-GPS0
RX-GPS0

TP1
Testpoint

R19
Res3
100k
311-100KHRCT-ND

Q1
BSS138
BSS138CT-ND

GPS-RESET
D3

RX/TX not crossed here

C13
Cap Pol3
4.7uF
478-3120-1-ND

C14
Cap Pol3
4.7uF
478-3120-1-ND

C15
Cap Pol3
4.7uF
478-3120-1-ND

3.3V-GPS-BACKUP
3.3V-GPS

D2
R20
Res3
10k
311-10.0KHRCT-ND

296-38557-1-ND
LP5907MFX-3.3/NOPB
U8
5V
3.3V-GPS
TP2
Testpoint

C16
Cap Pol3
4.7uF
478-3120-1-ND

C19
Cap Pol3
4.7uF
478-3120-1-ND

296-12008-1-ND
TPS71533DCKR
U9
TP3
Testpoint

C17
Cap Pol3
4.7uF
478-3120-1-ND

C18
Cap Pol3
4.7uF
478-3120-1-ND

GND

Title		
Size: Letter	Number	Revision
Date: 4-09-2021		Sheet of
File: K:\OneDrive\..\gps.SchDoc		Drawn By:

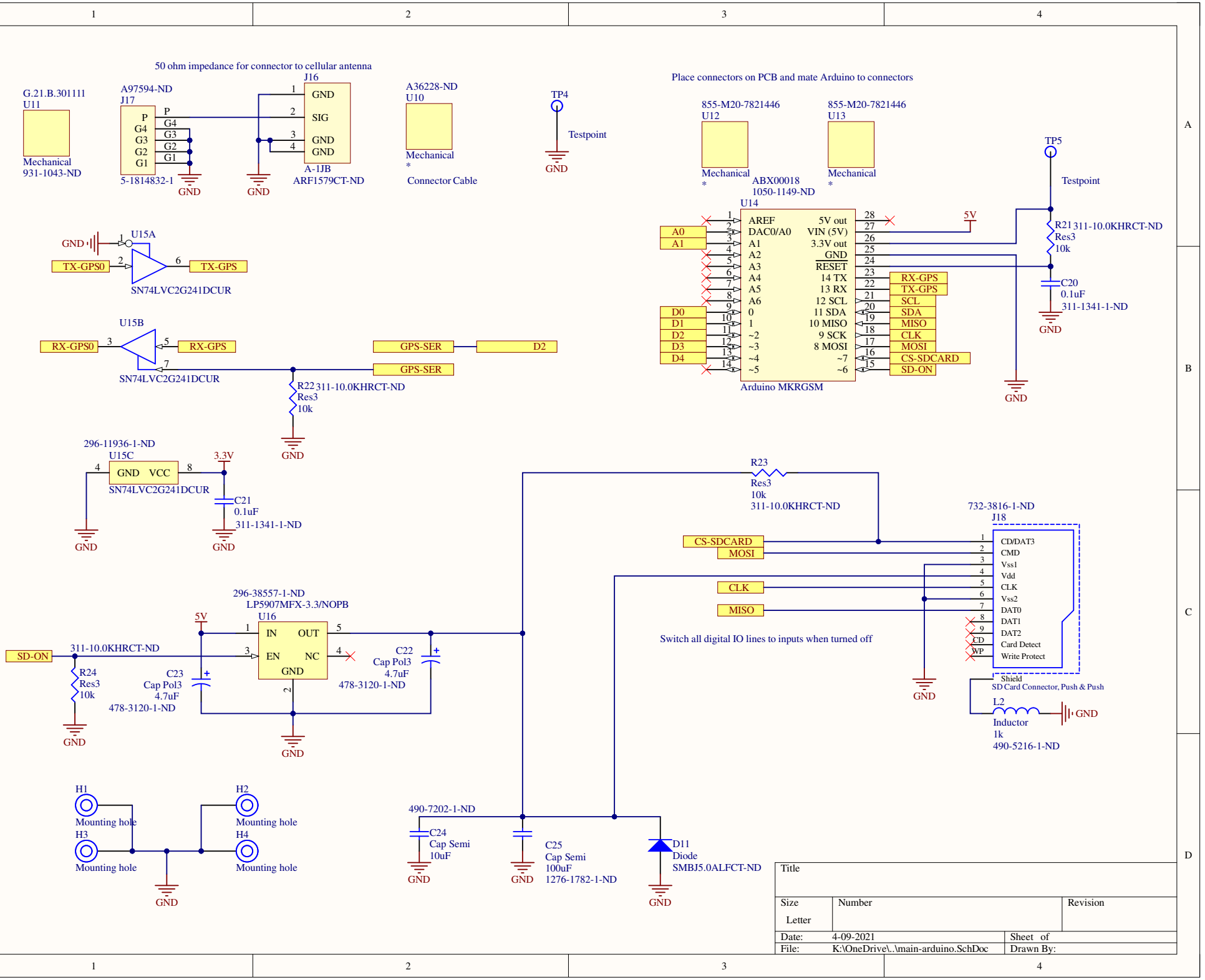
50 ohm impedance for connector to cellular antenna
G.21.B.301111
U11
Mechanical
931-1043-ND
A97594-ND
J17
P
G4
G3
G2
G1
5-1814832-1
J16
GND
SIG
GND
GND
A-1JB
ARF1579CT-ND
A36228-ND
U10
Mechanical
*
Connector Cable
TP4
Testpoint
GND
Place connectors on PCB and mate Arduino to connectors
855-M20-7821446
U12
Mechanical
*
855-M20-7821446
U13
Mechanical
*
ABX00018
1050-1149-ND
U14
AREF
DAC0/A0
A1
A2
A3
A4
A5
A6
0
1
~2
~3
~4
~5
5V out
VIN (5V)
3.3V out
GND
RESET
14 TX
13 RX
12 SCL
11 SDA
10 MISO
9 SCK
8 MOSI
~7
~6
A0
A1
D0
D1
D2
D3
D4
RX-GPS
TX-GPS
SCL
SDA
MISO
CLK
MOSI
CS-SDCARD
SD-ON
Arduino MKRGSM
5V
TP5
Testpoint
R21
311-10.0KHRCT-ND
Res3
10k
C20
0.1uF
311-1341-1-ND
GND
U15A
GND
TX-GPS0
TX-GPS
SN74LVC2G241DCUR
U15B
RX-GPS0
RX-GPS
SN74LVC2G241DCUR
GPS-SER
D2
GPS-SER
R22
311-10.0KHRCT-ND
Res3
10k
GND
296-11936-1-ND
U15C
GND
VCC
SN74LVC2G241DCUR
3.3V
C21
0.1uF
311-1341-1-ND
GND
GND
R23
Res3
10k
311-10.0KHRCT-ND
732-3816-1-ND
J18
CD/DAT3
CMD
Vss1
Vdd
CLK
Vss2
DAT0
DAT1
DAT2
CD
WP
Card Detect
Write Protect
Shield
SD Card Connector, Push & Push
CS-SDCARD
MOSI
CLK
MISO
Switch all digital IO lines to inputs when turned off
GND
L2
Inductor
1k
490-5216-1-ND
GND
296-38557-1-ND
LP5907MFX-3.3/NOPB
U16
IN
OUT
EN
NC
GND
5V
SD-ON
311-10.0KHRCT-ND
R24
Res3
10k
C23
Cap Pol3
4.7uF
478-3120-1-ND
C22
Cap Pol3
4.7uF
478-3120-1-ND
GND
GND
H1
Mounting hole
H2
Mounting hole
H3
Mounting hole
H4
Mounting hole
GND
490-7202-1-ND
C24
Cap Semi
10uF
C25
Cap Semi
100uF
1276-1782-1-ND
D11
Diode
SMBJ5.0ALFCT-ND
GND
GND
GND
Title
Size
Letter
Number
Revision
Date:
4-09-2021
Sheet of
File:
K:\OneDrive\..\main-arduino.SchDoc
Drawn By:

5V Power Supply

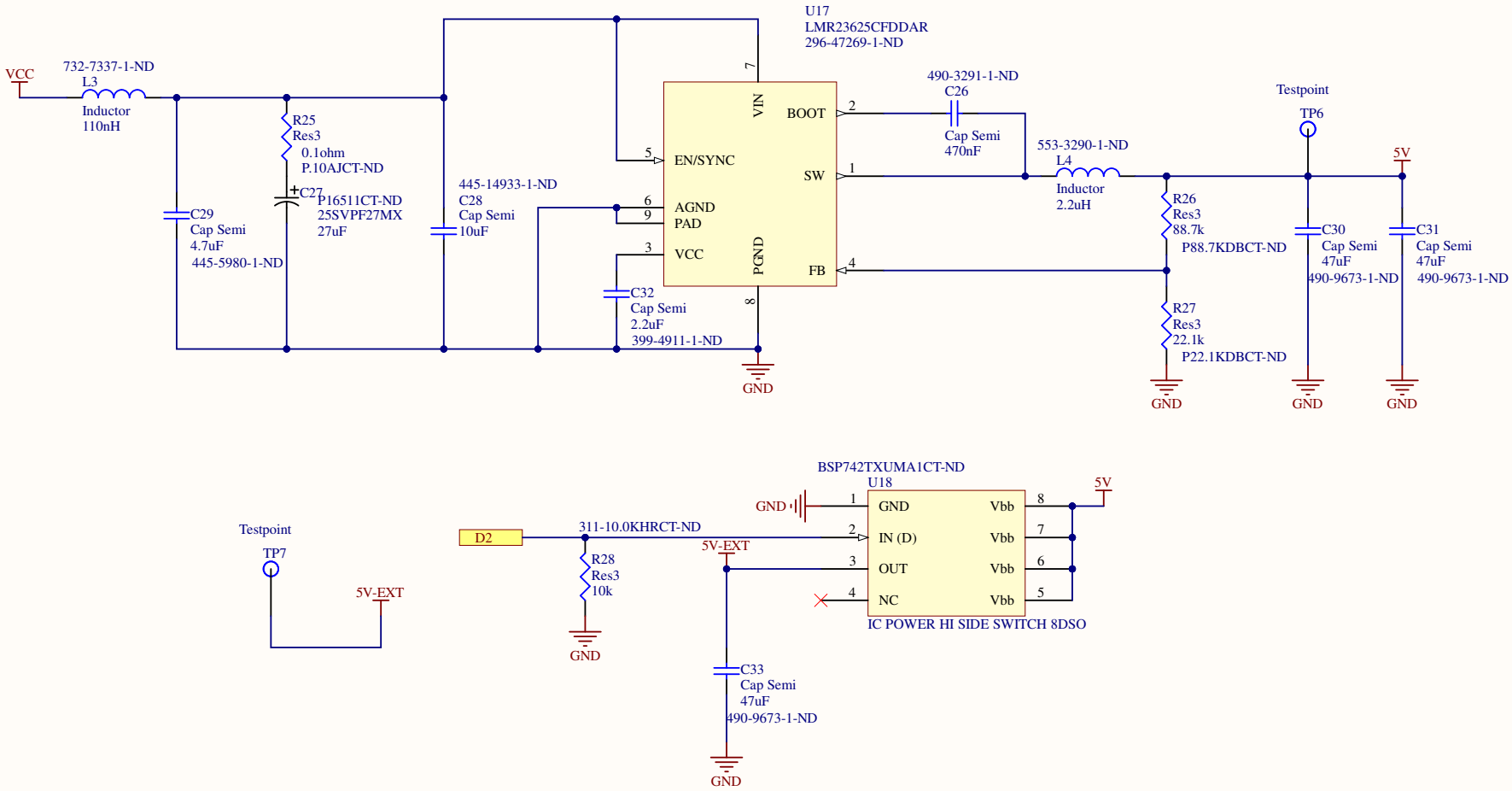

Title		
Size: Letter	Number	Revision
Date: 4-09-2021		Sheet of
File: K:\OneDrive\..\main-power.SchDoc		Drawn By:

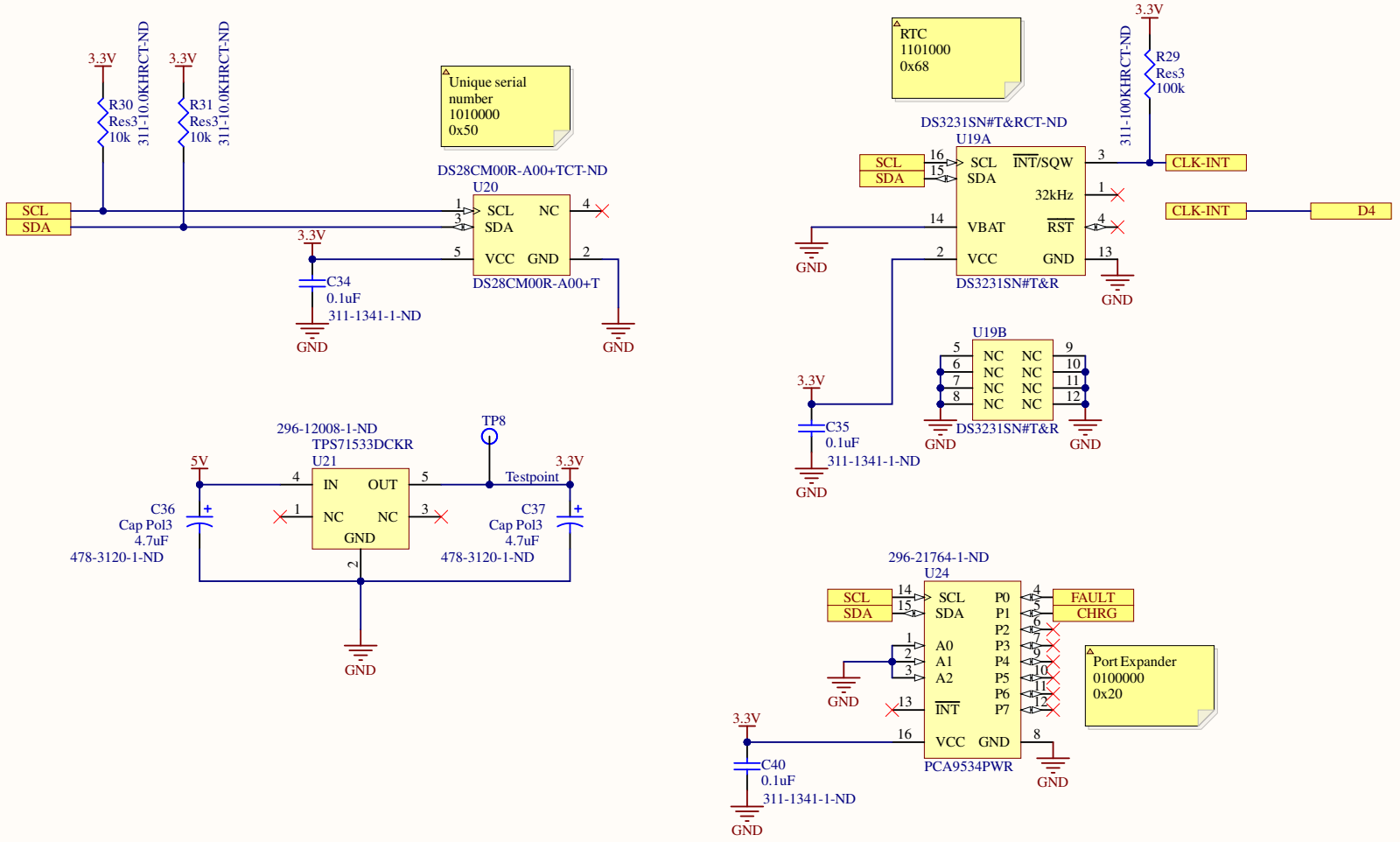

Title		
Size: Letter	Number	Revision
Date: 4-09-2021		Sheet of
File: K:\OneDrive\..\rtc.SchDoc		Drawn By:

Figures

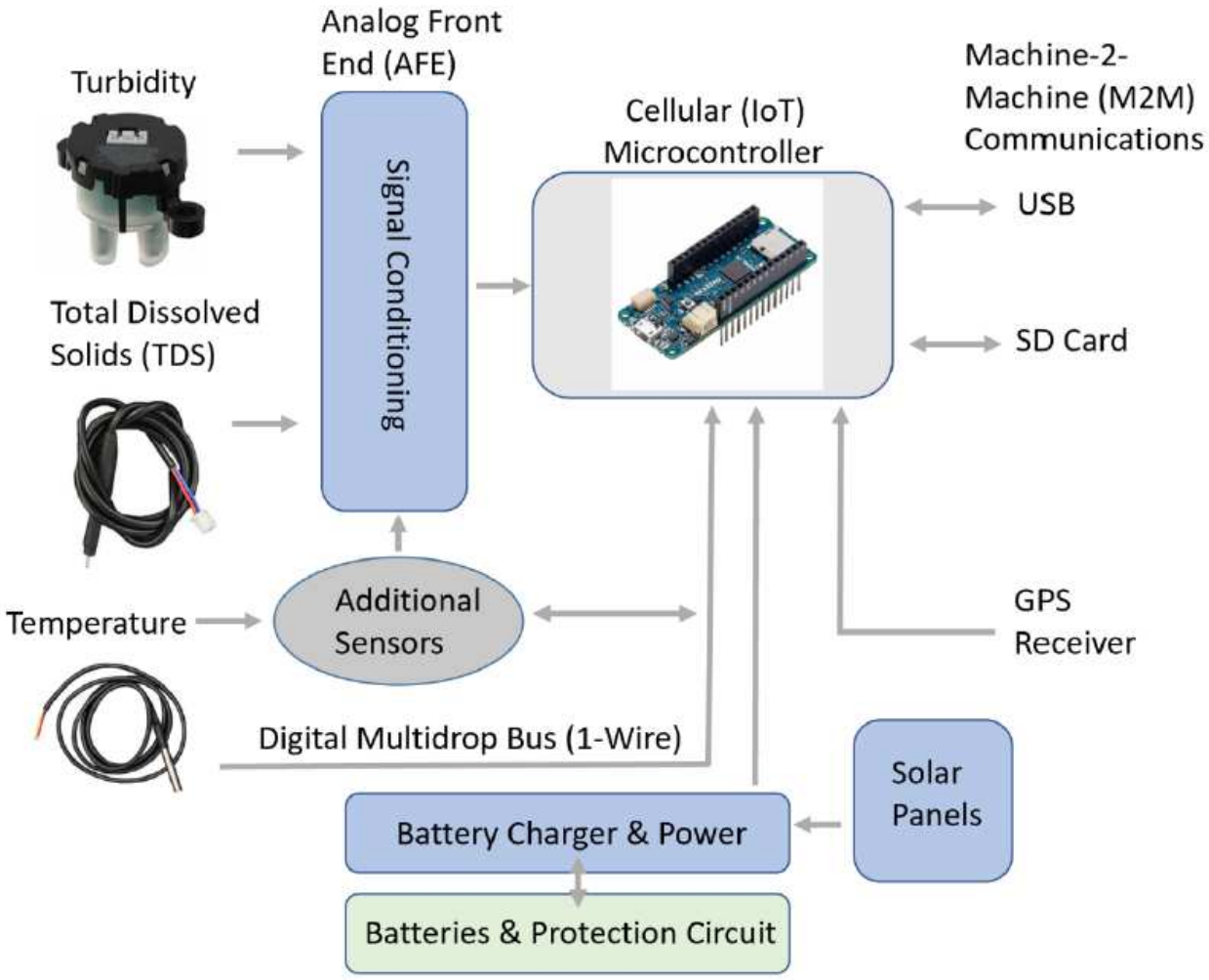

Figure 1

Block diagram of WaterWatcher system showing sub-systems. Photographs courtesy Digikey Incorporated (Thief River Falls, Minnesota, USA) and are used with permission.

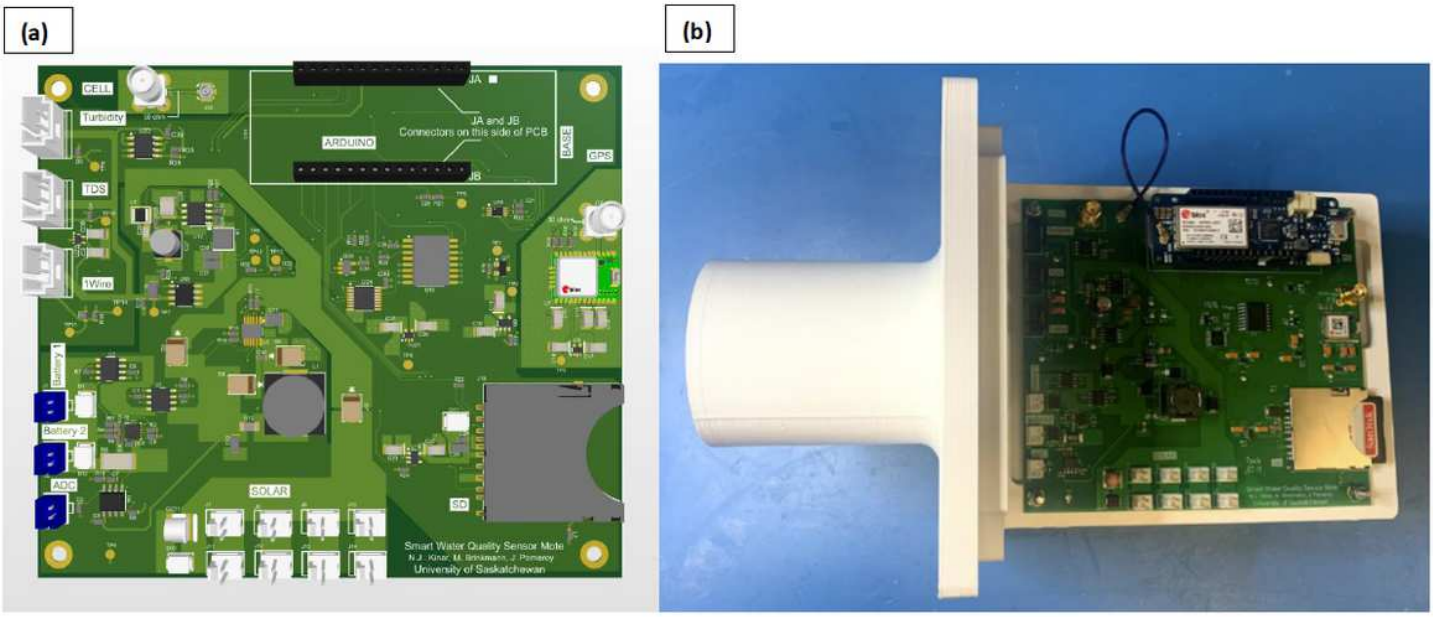

Figure 2

(a) 3D rendering of the electronic printed circuit board (PCB) for the WaterWatcher system. System components are labeled on the PCB. (b) Picture of constructed PCB mounted with mechanical fasteners on a 3D printed plastic part.

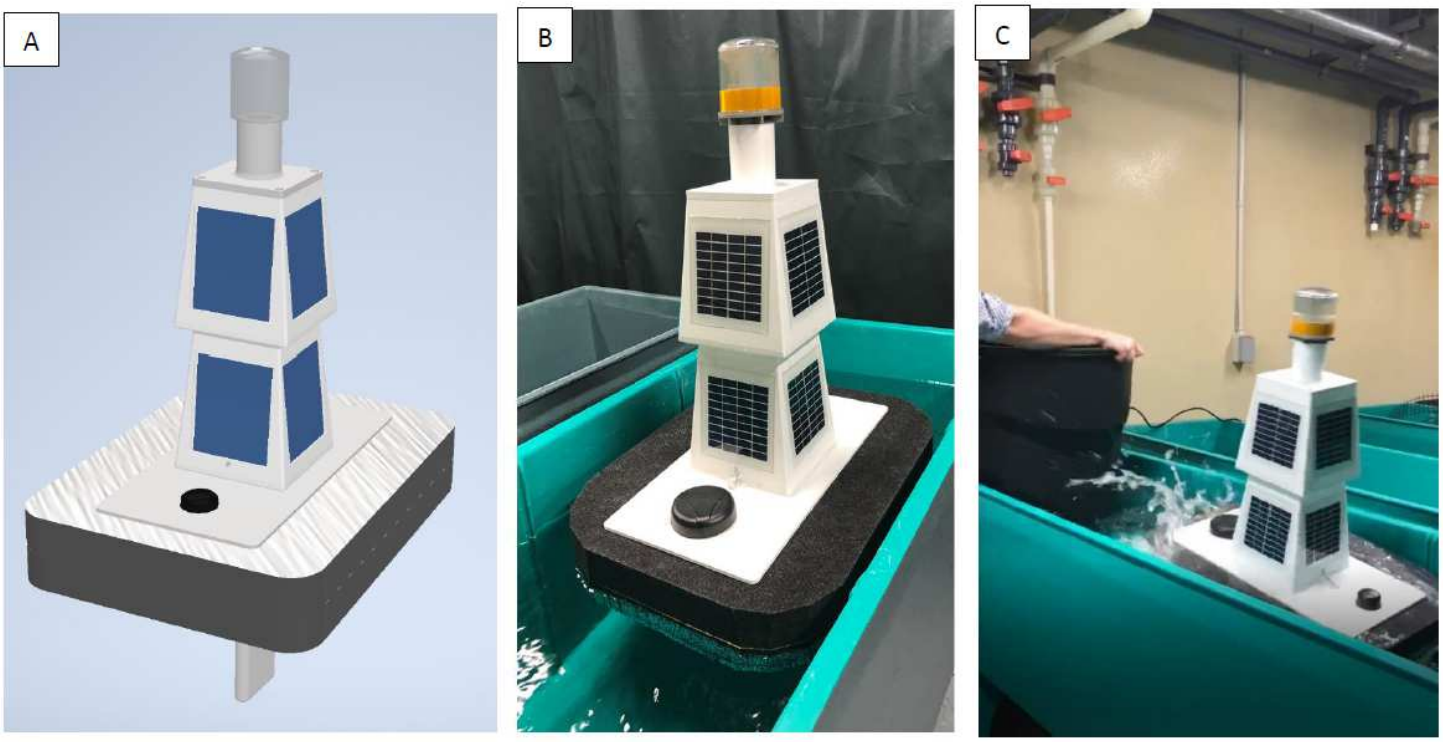

Figure 3

(a) CAD software rendering of mechanical WaterWatcher enclosure. The 3D model includes all mechanical parts that comprise the system. (b) Actual photograph of the WaterWatcher system tested in

a tank. (c) Photograph of tank test to check for buoyancy and stability.

Figure 4

Deployment of WaterWatcher at an urban reservoir (Aspen Ridge Forebay, City of Saskatoon, Saskatoon, Saskatchewan, Canada).

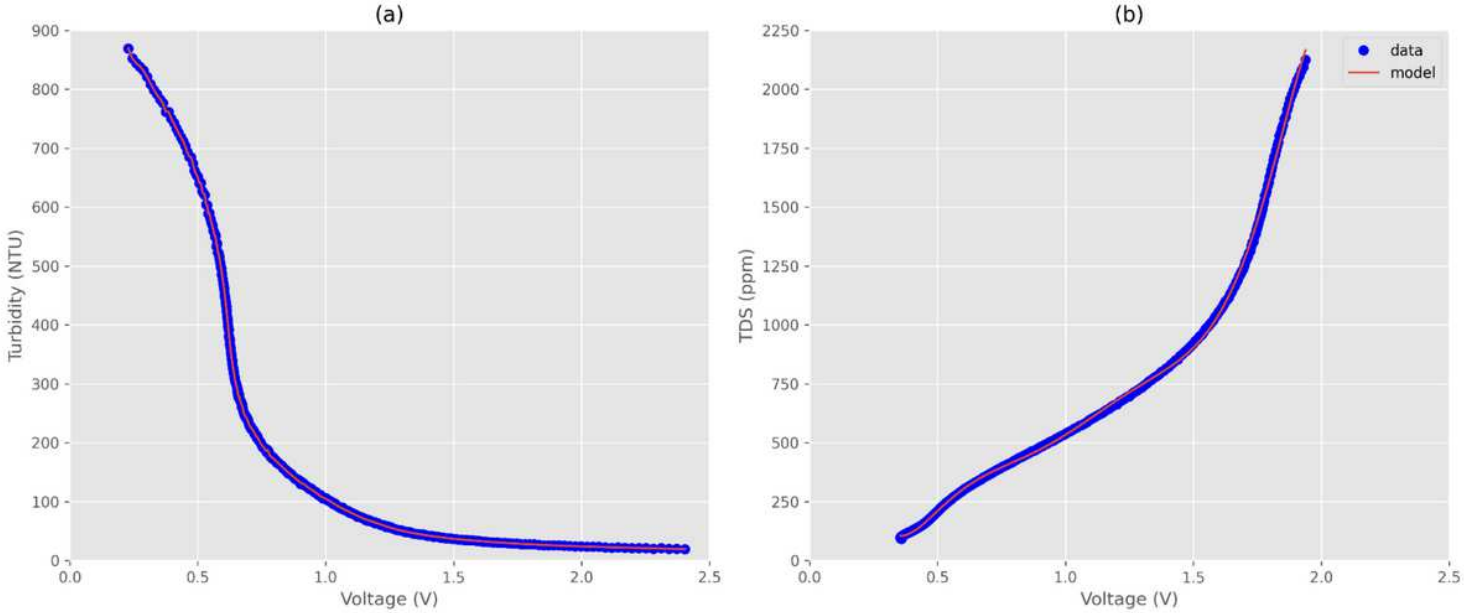

Figure 5

Calibration experiments to relate sensor output voltages to (a) turbidity and (b) TDS. The data are shown as circle markers, whereas the model is shown as a line on each plot.

Figure 6

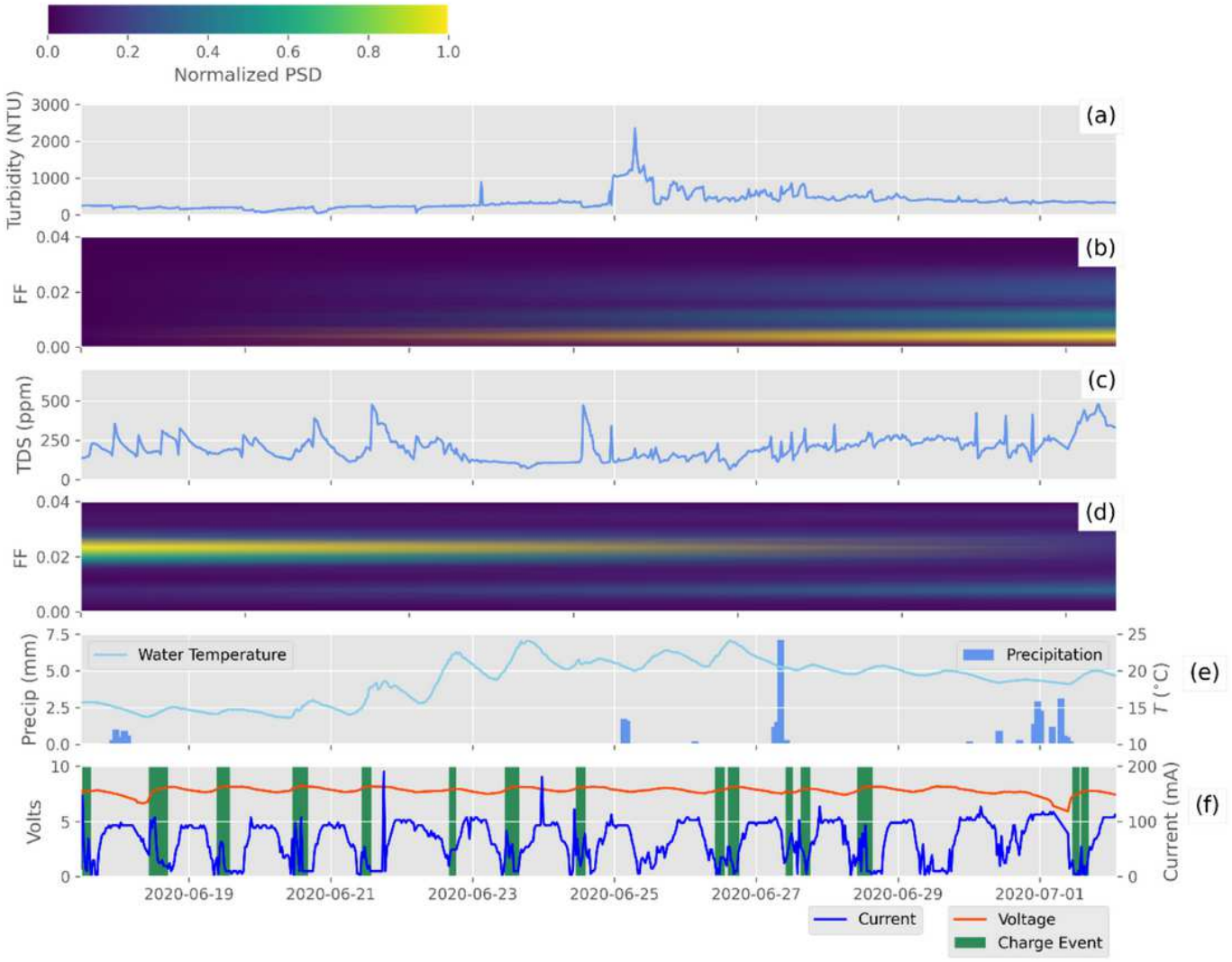

Field data collected at the Aspen Ridge Forebay location. (a) Turbidity time series; (b) spectrogram of turbidity time series with fractional frequency (FF); (c) TDS time series; (d) spectrogram of TDS time series with fractional frequency (FF); (e) precipitation events as measured at Saskatoon by Environment and Climate Change Canada along with reservoir water temperature T (˚C) ; (f) time series of battery voltage showing discrete battery charging events associated with operation of the solar panel battery charger and battery current consumption. As shown by the colorbar at the top of the figure, the spectrogram Power Spectral Density (PSD) has been normalized with respect to the maximum power of the time series signals associated with spectrograms (b) and (d).

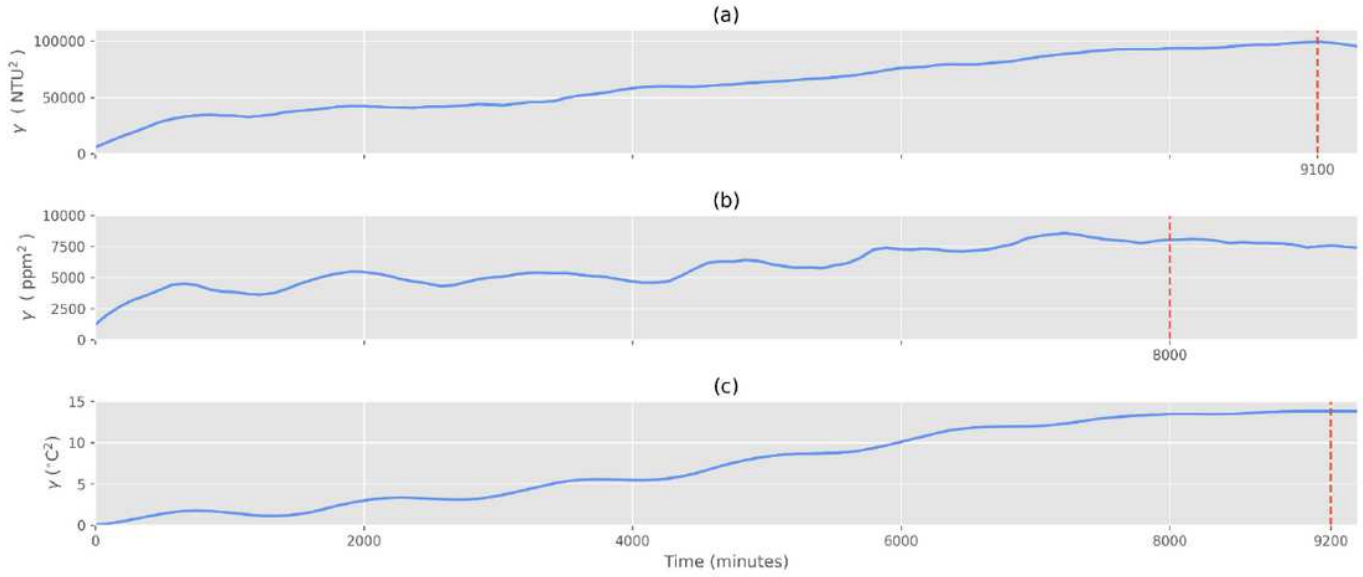

Figure 7

Semivariance γ of (a) turbidity, (b) TDS and (c) water temperature time series. The range is marked on the x-axis as a vertical dashed line to indicate temporal autocorrelation at time intervals less than the range.